

Twenty-year monitoring of the surface magnetic fields of chemically peculiar stars

M. Giarrusso^{1,2}, M. Cecconi³, R. Cosentino³, M. Munari², A. Ghedina³, F. Ambrosino⁴,
W. Boschin^{3,5,6}, F. Leone^{7,2}

¹Department of Physics and Astronomy, University of Florence, Largo Enrico Fermi 2, 50125, Firenze, Italy

²INAF - Osservatorio Astrofisico di Catania, Via S. Sofia 78, I-95123 Catania, Italy

³INAF - Fund. Galileo Galilei, Rambla José Ana Fernández Perez 7, 38712 Breña Baja (La Palma), Canary Islands, Spain

⁴INAF - Osservatorio Astrofisico di Roma, Via Frascati 33, I-00078, Monteporzio Catone (Roma) Italy

⁵Instituto de Astrofísica de Canarias (IAC), Calle Vía Láctea s/n, 38205 La Laguna, TF - Spain

⁶Departamento de Astrofísica, Universidad de La Laguna (ULL), 38206 La Laguna, TF - Spain

⁷Università di Catania, Dipartimento di Fisica e Astronomia, Sezione Astrofisica, Via S. Sofia 78, I-95123 Catania, Italy

Received To be inserted later, accepted To be inserted later

ABSTRACT

Magnetic chemically peculiar stars of the main sequence can present rotational periods as long as many decades. Here we report the results of an observational campaign started in 2001 aimed at establishing these very long periods from the variability of the integrated magnetic field modulus, the so-called surface magnetic field B_s , as measured from the Zeeman splitting of the FeII 6149.258 Å spectral line. Thirty-six stars have been monitored with various high-resolution spectrographs at different telescopes, totalling 412 newly collected spectra. To improve the phase coverage, we have also exploited all public archives containing high-resolution spectra, many not yet published. On the basis of these new B_s variability curves, we 1) confirm or revisit the periods of 24 stars, 2) extend the lower limits to the periods of HD 55719 ($P > 38$ yr), HD 165474 ($P > 27$ yr), HD 177765 ($P > 37$ yr), 3) establish for the first time the periods of HD 29578 ($P = 10.95$ yr), HD 47103 ($P = 17.683$ d), HD 150562 ($P = 5.7$ yr), HD 216018 ($P = 34.044$ d), and 4) set lower limits to the periods of HD 75445 ($P >> 14$ yr), HD 110066 ($P >> 29$ yr), HD 116114 ($P > 48$ yr), and HD 137949 ($P > 27$ yr). As to γ Equ, whose period must exceed 90 years, we point out a clear decrease in the field modulus, the maximum of which coincides within the uncertainties with the minimum of the variation in the integrated longitudinal field.

Key words: Plasmas, Magnetic fields, Line: formation, Line: profiles, Techniques: spectroscopy, Stars: magnetic fields

1 INTRODUCTION

Following initial measurements of the surface magnetic field B_s (average of the magnetic field modulus over the visible stellar disk) of the star HD 215441 by Babcock (1960), large numbers of B_s measurements in Magnetic Chemically Peculiar (MCP) stars have been reported by Preston (1971), Mathys et al. (1997) (=M97) and Mathys (2017) (=M17). These days, the most straightforward and accurate method to determine B_s is based on the Zeeman splitting of the FeII 6149.258 Å spectral line which features two Zeeman π subcomponents coinciding with two σ subcomponents (Mathys 1990).

Within the framework of the oblique rotator model first proposed by Babcock (1949) and further developed by Stibbs (1950), MCP stars present photometric, spectroscopic, and magnetic variability with a single period as a consequence of stellar rotation. Measuring the rotational period from the modulation of the surface

magnetic field is probably the most reliable approach to the study of very long-term variations. All the necessary information is embedded in a single spectrum and there is no need for standard stars or zero point adjustments as in the case of photometry.

This paper reports the results of an observational campaign started in 2001 to measure and monitor the surface fields of 36 MCP stars whose rotational periods were expected to be very long, up to decades, judging from the sharpness of their spectral lines. As indicated above, field measurements rely on high-resolution spectra of the FeII 6149.258 Å line. In order to extend as much as possible the time frame, we have in addition explored all public astronomical archives and mined the literature. We have also analysed some of our spectra dating back to 1995.

In Section 2, we present the: 1) high-resolution spectrographs we have operated, 2) reduction methods, 3) procedure to measure B_s from the FeII 6149.258 Å spectral line, and 4) method to estab-

Table 1. List of spectrographs used to measure stellar surface magnetic fields together with the spectral resolution $R[k] = \frac{\lambda}{\Delta\lambda}/1000$. For every instrument, N represents the number of B_s measurements from spectra acquired in this study. A two-letter identification is used for the instruments.

Spectrograph@Telescope		R [k]	N	Reference
CAOS@OAC	CS	55	123	Leone et al. (2016)
HARPS@ESO 3.6m	HS	115	20	Mayor et al. (2003)
HARPS-North@TNG	HN	115	81	Cosentino et al. (2013)
UCLES@AAT	UC	120	22	Horton et al. (2012)
SARG@TNG	SG	≤ 164	53	Gratton et al. (2001)
CES@ESO 3.6m	CE	220	2	Enard (1982)

Table 2. Archives hosting high-resolution spectra of long period magnetic chemically peculiar stars. For every instrument, N represents the number of B_s measurements from archive spectra.

Spectrograph@Telescope		R [k]	N	Reference
ELODIE@OHP-1.9m	EE	40	6	Baranne et al. (1996)
FEROS@ESO-2.2m	FS	48	6	Kaufer et al. (1999)
EMMI@ESO-NTT	EM	60	2	D’Odorico (1990)
NES@BTA	NS	60	6	Panchuk et al. (2009)
ESPaDOs@CFHT	ES	65	85	Silvester et al. (2012)
NARVAL@TBL	NL	65	16	Silvester et al. (2012)
UCLES@AAT	UC	90	10	Horton et al. (2012)
UVES@ESO-UT2	US	100	72	Dekker et al. (2000)
HARPS@ESO-3.6m	HS	115	350	Mayor et al. (2003)
GECKO@CFHT	GO	120	21	Glaspey (1993)
CES@ESO-3.6m	CE	220	7	Enard (1982)

lish the variability period. In Section 3, we present the rotational periods star-by-star. Whenever possible, these periods have been checked with the effective magnetic field B_e (average over the visible stellar disk of the magnetic field component along the line of sight) and/or photometric results, or determined from a combination of these data. Finally, we present an empirical relation between rotational period and magnetic field strength.

2 OBSERVATIONS, ARCHIVES, DATA REDUCTION AND PERIOD SEARCH

We have carried out high-resolution spectroscopy of 36 MCP stars with the instruments listed in Table 1, for a total of 412 newly acquired spectra. The data have been reduced using IRAF routines as described in Leone et al. (2017). To extend as much as possible the time frame for determining the variability periods we have exploited all public archives storing high-resolution spectra (Table 2) with the FeII 6149.258 Å line. A total of 581 spectra have been retrieved.

Following Mathys (1990, 2017) and Mathys et al. (1997), measurements of the surface magnetic field B_s have been derived (assuming a linear Zeeman effect regime) from the distance $\Delta\lambda$ between the Zeeman subcomponents of the FeII 6149.258 Å line:

$$B_s[G] = 20974\Delta\lambda[\text{\AA}] \quad (1)$$

The wavelengths of Zeeman subcomponents have been obtained with a double Gaussian fit (top panel of Figure 1). The error in a surface magnetic field measurement results from the propagation of errors in the determination of subcomponent positions. In the case of stars, e.g. HD 9996, with a blend of the FeII 6149.258 Å and not yet identified, ~ 6148.84 Å spectral lines, the previous 2 Gaussians

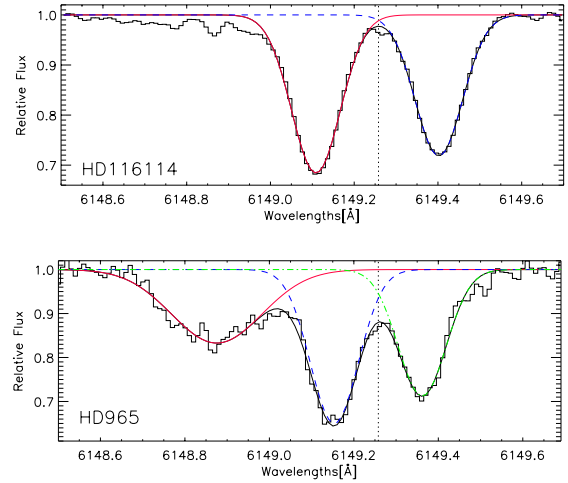


Figure 1. The distance between the Zeeman subcomponents of the FeII 6149.258 Å line is determined via (a) a double Gaussian fit or (b) a triple Gaussian fit including the yet unidentified spectral line at ~ 6148.84 Å.

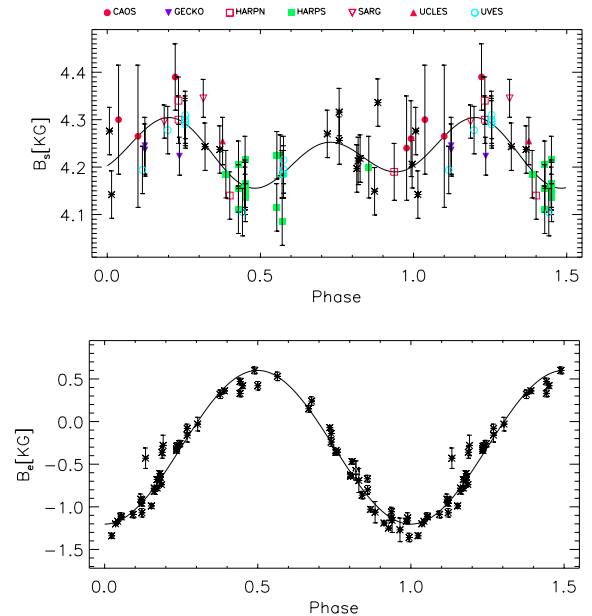


Figure 2. HD 965. B_s and B_e variations, folded with the 6030 d period.

have been assumed identical in width, and a 3rd Gaussian component has been added (bottom panel of Figure 1).

In this paper, the measurements of the surface magnetic field by Mathys et al. (1997) (=M97) and Mathys (2017) (=M17) are fundamental. The huge observational effort of these authors represents a significant enlargement of the time base for many stars. Whenever it was possible, we retrieved the original spectroscopic data of these authors and derived the surface magnetic field. On average, our measurements are 50 G smaller than Mathys’ values. For this reason, when original spectra of Mathys and coworkers were not available, we have combined B_s values published by M97 and M17 with our values after the application of this shift.

Variability periods are determined here from the Lomb-Scargle (Press & Rybicki 1989) periodogram of the surface mag-

Table 3. Observed stars. Literature and adopted ephemerides of B_s variability.

HD / HDE	Other id.	$T_{\text{eff}}[K] / R[R_{\odot}]$	Literature Ephemeris		Reference	Here determined or adopted Ephemeris	
			JD = 2400000+	Period (days)		$HJD_0 = 2400000+$	Period (days)
965	BD −00 21	7027 / 2.46	$B_e^{\min} = 51000.0$	6030 ± 200	Mathys et al. (2019b)	$B_e^{\min} = 51000.0$	6030
2453	BD +31 59	8355	$B_e^{\min} = 42213.0$ $c_1^{\max} = 48440.911$	521 ± 2 518.2 ± 0.5	Mathys (2017) Pyper & Adelman (2017)	$B_e^{\min} = 48440.911$	518.2
9996	HR 465	9200	$y^{\max} = 53016.610$ $B_e^{\min} = 33301.360$	7850 ± 100 7936.522	Pyper & Adelman (2017) Bychkov et al. (2019)	$B_s^{\max} = 49200.0$	7850
12288	BD +68 144	8415	$B_e^{\max} = 48499.87$ $v^{\max} = 51131.772$ $V^{\max} = 57218.6$	34.9 ± 0.2 34.99 ± 0.01 35.73 ± 0.2	Wade et al. (2000b) Pyper & Adelman (2017) Bernhard et al. (2020)	$B_e^{\max} = 51131.9$	34.993 ± 0.003
14437	BD +42 502	9660	$V^{\max} = 57077.7$ $B_e^{\max} = 48473.846$	26.78 ± 0.1 26.87 ± 0.02	Bernhard et al. (2020) Wade et al. (2000b)	$v^{\max} = 49228.820$	26.734 ± 0.007
18078	BD +55 726	7718 / 4.43	$B_s^{\max} = 49930.0$	1358 ± 12	Pyper & Adelman (2017) Mathys et al. (2016a)	$B_s^{\max} = 49916$	1352 ± 6
29578	CPD −54 685	7340 / 2.88		$>> 1800$	Mathys (2017)	$B_s^{\max} = 51950.0$	$4000 / 9370$
47103	BD +20 1508	8108		> 10	Wraight et al. (2012)	$B_s^{\max} = 50098.99$	17.683 ± 0.004
50169	BD −1 1414	8901		10600 ± 300	Mathys et al. (2019a)	$B_s^{\max} = 41600.0$	10600
51684	CoD −40 2796	7546 / 2.99	$B_s^{\max} = 49947.0$	371 ± 6	Mathys et al. (2019a)	$B_s^{\max} = 53617$	366 ± 1
55719	HR 2727	9131		$>> 3650$	Mathys (2017)	48500	≥ 14000
61468	CoD −27 4341	9057	$B_e^{\max} = 50058.5$	322 ± 3	Mathys (2017)	$B_e^{\max} = 50058.5$	321 ± 1
75445	CoD −38 4907	9057		6.291 ± 0.002 ?	Mathys (2017)		> 5000
81009	HR 3724	8430	$v^{\min} = 48646.878$ $v^{\max} = 44483.420$	33.987 ± 0.002 33.984 ± 0.055	Pyper & Adelman (2017) Wade et al. (2000c)	$B_s^{\max} = 48645.9$	33.987
93507	CoD −67 1494	8999	$B_e^{\min} = 49800.0$	556 ± 22	Mathys et al. (1997)	$B_s^{\max} = 48965.0$	562 ± 5
94660	HR 4263	9571	$B_s^{\min} = 47000.0$	2800 ± 200	Mathys (2017)	$B_s^{\max} = 48284.0$	2830 ± 140
110066	HR 4816	8878	phot. not variable $B_s^{\min} = 49826.738$	6.4769 ± 0.0011	Pyper & Adelman (2017) Bychkov et al. (2021)		$> 10\,500$
116114	BD −17 3829	7424 / 2.84	$m^{\max} = 54352.057$ $B_e^{\max} = 47539.000$	5.3832 27.61	Wraight et al. (2012) Mathys (2017)	$B_s^{\max} = 40350.0$	> 17700
126515	BD +1 2927	9422	$B_e^{\max} = 37015.000$ $v^{\min} = 52031.708$	129.95 129.95 ± 0.02	Mathys (2017) Pyper & Adelman (2017)	$B_e^{\max} = 37015.0$	129.95
137949	33 Lib	7406 / 1.97	many decades phot. not variable $B_e^{\max} = 38166$	5195	Landstreet et al. (2014) Pyper & Adelman (2017) Mathys (2017)		$> 10\,000$
142070	BD −0 3026	8130	$v^{\min} = 50837.499$ $B_e^{\max} = 49878.2$	3.37189 ± 0.00007 3.3718 ± 0.0011	Adelman (2001) Mathys (2017)	$B_e^{\max} = 49878.2$	$B_e^{\max} = 3.3721 \pm 0.0002$
144897	CoD −40 10236	7398 / 2.89	$B_e^{\max} = 49133.7$	48.57 ± 0.15	Mathys (2017)	$B_e^{\max} = 491157.1$	48.60 ± 0.02
150562	CoD −48 11127	6390 / 2.13		> 1600	Mathys (2017)	$B_e^{\max} = 54317.0$	2100 ± 200
154708	CD −57 6753	6812 / 1.66	$B_e^{\max} = 54257.740$	5.363 ± 0.003	Landstreet et al. (2014)	$B_e^{\max} = 53662.57$	5.367 ± 0.001
318107	CoD −32 13074	9050	$B_e^{\max} = 48800.000$	9.7088 ± 0.0007	Bailey et al. (2011)	$B_e^{\max} = 48800.0$	9.7089 ± 0.0002
165474	BD +12 3382	7692 / 2.82		$>> 3300$	Mathys (2017)	$B_e^{\max} = 52150.0$	≥ 9900
166473	CoD −37 12303	7451 / 1.88	$B_s^{\max} = 48660.0$	3836 ± 30	Mathys et al. (2020)	$B_s^{\max} = 48660.0$	3836
177765	CoD −26 13816	7002 / 3.52		$>> 1800$	Mathys (2017)		≥ 13500
178892	BD +14 3811	7582 / 2.06	$V^{\max} = 52708.562$	8.2549	Semenko et al. (2011)	$B_s^{\max} = 52696.850$	8.2572 ± 0.0016
187474	HR 7552	9438	$B_e^{\min} = 46766.000$	2345	Mathys (2017)	$B_s^{\max} = 57176$	2324 ± 40
188041	HR 7575	8400	$v^{\min} = 49904.860$ $B_e^{\max} = 46319.5$	223.826 ± 0.040 223.78 ± 0.10	Pyper & Adelman (2017) Mathys (2017)	$B_e^{\max} = 49797.921$	223.826
192678	BD +53 2368	9276	$B_e^{\max} = 44890.170$	6.4193 ± 0.003	Pyper & Adelman (2017)	$B_s^{\max} = 49112.76$	6.4199 ± 0.0001
335238	BD +29 4202	9045	47000	48.7 ± 0.1	Mathys (2017)	$B_e^{\max} = 57222.7$	48.985 ± 0.007
201601	γ Equ	7457 / 2.16	$B_e^{\min} = 52457.1$	35462.5 ± 1149	Bychkov et al. (2016)	$B_e^{\max} = 52200.0$	35462.5
208217	CPD −62 6281	8140	$B_e^{\max} = 47028.0$	8.44475 ± 0.00011 8.317 ± 0.001	Mathys (2017) David-Uraz et al. (2019)	$B_s^{\max} = 47027.094$	8.445 ± 0.005
216018	BD −12 6357	7719 / 2.08		> 10 $>> 2000$	Wraight et al. (2012) Mathys (2017)	$B_e^{\max} = 49531.870$	34.044 ± 0.007

netic field measurements: $LS(B_s)$. If necessary, the periodograms of other observables ($LS(O^i)$) have also been computed and the final period determined as the position of the highest peak in the product: $LS(B_s, O^1, O^2, \dots) = \frac{LS(B_s)}{LS^{max}(B_s)} \times \prod_i \frac{LS(O^i)}{LS^{max}(O^i)}$. We assume that spurious peaks in the respective periodograms – due to data sampling and noise – of these observables do not coincide and that they cancel or at least are greatly reduced in the product. Normalisation of any periodogram to its maximum value is equivalent to assuming equal weight for all datasets.

Estimating the uncertainty in the determination of periods has always proved a controversial subject; the literature abounds with proposed methods that we might choose for this purpose. [Pyper & Adelman \(2017\)](#) (=P17) – many of their stars are in common with our sample – wrote: “we used the practical method of comparing the two good data sets most widely separated in time and determined how much the period had to be changed to see a definite shift in phase”. Whereas [Mathys et al. \(2019b\)](#) state that “by plotting a phase diagram of the measurements for a series of tentative values of the period around the one suggested by the periodogram, one can visually identify the period value that minimizes the phase shifts between field determinations from different rotation cycles, and constrain the range around that value for which those phase shifts remain reasonably small”. We prefer to adopt a “clinical” decision based on the σ value of a Gaussian fit to the highest peak in the periodogram as a measure of the uncertainty in the period determination. If our period coincides within errors with the value quoted in the literature and if the latter has been determined to within a smaller error, we have adopted the period taken from the literature.

3 INDIVIDUAL STARS

Table 3 lists the 36 MCP stars discussed in this paper, listing the ephemerides taken from the literature and the ones adopted here. For every star, from Table 6 to 41, measured surface field values are given together with estimated errors, Heliocentric Julian Date (HJD) and the spectrographs used – as coded in Tables 1 and 2. Field measurements by Mathys and coworkers are indicated with asterisks in the figures shown hereafter. When data taken from the literature are used, sources and symbols are detailed in the corresponding subsection and figures, respectively. If different photometric data sets are available for a star, these are overplotted after the application of an ad hoc shift.

In a similar way to M17, B_s measurements folded with the variability period are fitted (by the CURVEFIT routine of Interactive Data Language Version 8) with the trigonometric function

$$B_s = B_0 + B_1 \sin(2\pi(\phi + \phi_1))$$

or the function

$$B_s = B_0 + B_1 \sin(2\pi(\phi + \phi_1)) + B_2 \sin(2\pi(2\phi + \phi_2))$$

where $\phi = \frac{HJD - HJD_0}{P}$ is the phase, the zero phase time HJD_0 and period P are from Table 3. Measurements are weighted by the inverse of the square of uncertainty. Fit coefficients are listed in Table 4.

3.1 HD 965

[Mathys et al. \(2019b\)](#) noted that B_s measurements of HD 965, collected between 1993 and 2008, do not show significant variations.

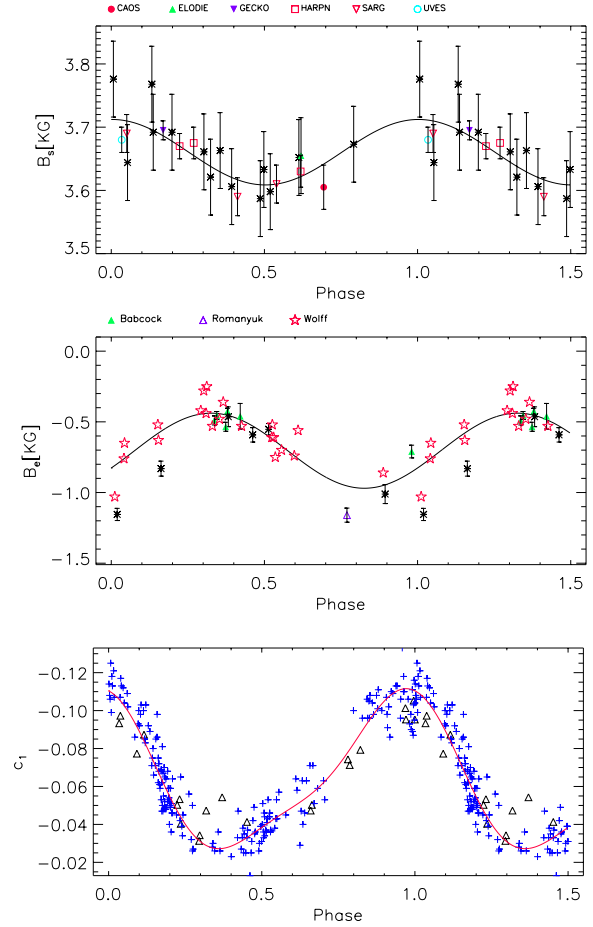


Figure 3. HD 2453. B_s , B_e and c_1 index variability, folded with the 518.2 d period. c_1 values are from [Wolff \(1975\)](#) (+) and [Pyper & Adelman \(2017\)](#) (Δ).

In contrast, these authors found B_e measurements, collected between 1995 and 2017, to be variable with a period of 6030 ± 200 d. We have obtained high-resolution spectra of HD 965 between 2001 and 2021, and have retrieved spectra from the CFHT and ESO archives. The list of our B_s measurements of HD 965 is given in Table 6. There is no clear evidence for a periodically variable surface magnetic field: the average value is $\langle B_s \rangle = 4240 \pm 70$ G, where the r.m.s. is comparable to the error of single field measurement. However, B_s measurements folded with the period applicable to B_e (Table 3) present a double wave variation suggesting minima in coincidence with the extrema of the effective magnetic field, and maxima corresponding to zero B_e values (Fig. 2). The phase relations hint at a magnetic field that is certainly not purely dipolar.

3.2 HD 2453

Two periods have almost simultaneously been published for the variability of HD 2453: 1) 521 ± 2 d by M17 from B_e measurements and 2) 518.2 ± 0.5 d by P17 from Strömgren photometry. Our B_s measurements of HD 2453 (Table 7) extend the 2700 day coverage by M17 to 11000 days. However, with an average value of $B_s = 3690 \pm 60$ G and a scatter comparable to the error of a single field measurement, it is not possible to ascertain a clear variability of the surface magnetic field. The single $B_e = -1160 \pm 50$ G measurement obtained by [Romanyuk et al. \(2016\)](#) on JD = 2 455 075.417 makes

Table 4. Coefficients of a weighted fit of B_s (G) measurements with the function $B_0 + B_1 \sin\left(2\pi\left(\frac{HJD - HJD_0}{P} + \phi_1\right)\right) + B_2 \sin\left(2\pi\left(2\frac{HJD - HJD_0}{P} + \phi_2\right)\right)$. Period (P) and zero phase Heliocentric Julian Date (HJD_0) are from Table 3. $\chi^2 = \frac{1}{D_f} \sum_{i=1}^N w_i (B_i - B_{fit})^2$, where $D_f = N - M$ is the degrees of freedom (N is the number of measurements, and M is the number of coefficients) and the weight is equal to the inverse of the square of measurement uncertainty ($w_i = 1/\sigma_i^2$).

HD	B_0	B_1	ϕ_1	B_2	ϕ_2	N	χ^2
965	4229 ± 7	31 ± 11	0.161 ± 0.049	51 ± 10	0.792 ± 0.031	50	0.016
2453	3666 ± 7	32 ± 8	0.132 ± 0.067			21	0.056
9996	2759 ± 8	1680 ± 9	0.244 ± 0.001	537 ± 11	0.199 ± 0.002	24	0.875
12288	8065 ± 19	457 ± 29	0.497 ± 0.008	147 ± 25	0.283 ± 0.031	33	0.045
14437	7379 ± 30	388 ± 29	0.856 ± 0.014			40	0.146
18078	3395 ± 8	809 ± 12	0.253 ± 0.001			20	1.122
47103	17211 ± 20	397 ± 26	0.215 ± 0.012	241 ± 30	0.167 ± 0.018	11	0.539
50169	5059 ± 6	896 ± 10	0.239 ± 0.001	101 ± 7	0.271 ± 0.015	52	0.022
51684	6013 ± 5	271 ± 8	0.242 ± 0.004			13	0.222
61468	6720 ± 9	1122 ± 13	0.247 ± 0.001			13	0.559
81009	8373 ± 9	997 ± 11	0.245 ± 0.002			84	0.072
93507	7067 ± 13	317 ± 10	0.230 ± 0.010			59	0.052
94660	6218 ± 7	165 ± 8	0.247 ± 0.007			43	0.028
126515	12704 ± 11	3240 ± 12	0.240 ± 0.000			80	0.146
166473	7084 ± 9	1420 ± 12	0.247 ± 0.001			61	0.036
177765	3432 ± 6	107 ± 11	0.250 ± 0.015			11	0.175
178892	18889 ± 96	911 ± 92	0.649 ± 0.021			18	0.046
187474	5372 ± 3	632 ± 5	1.258 ± 0.001	231 ± 5	0.227 ± 0.003	45	0.111
188041	3596 ± 3	37 ± 5	0.155 ± 0.022			47	0.030
192678	4624 ± 6	103 ± 9	0.236 ± 0.014	39 ± 8	0.122 ± 0.035	42	0.060
335238	9357 ± 27	2064 ± 22	0.232 ± 0.003	977 ± 37	0.242 ± 0.004	36	0.140
201601	3444 ± 6	492 ± 8	0.258 ± 0.001			141	0.055
208217	7668 ± 48	587 ± 69	0.294 ± 0.018	417 ± 56	0.188 ± 0.020	44	0.053
216018	5570 ± 6	62 ± 10	0.233 ± 0.022			38	0.024

the 518.2 d period the most probable. The Lomb-Scargle analysis of B_e (from M17, Wolff (1975), Romanyuk et al. (2016)) and c_1 (from Wolff (1975), Pyper & Adelman (2017)) produces a $LS(B_s, B_e, c_1)$ peaking at 517.7 ± 1.8 d. We have adopted the P17 period to fold the B_s , B_e and c_1 data (Fig. 3). With this period, B_s presents a single wave variation that is in phase with the light curve and with a maximum coincident with the negative B_e extremum. This is what one can expect from a dominant dipole component of the magnetic field.

3.3 HD 9996

From B_e measurements, Metlova et al. (2014) and Bychkov et al. (2019) concluded at a variability period of HD 9996 of 7936.522 d (~ 21.7 yr). Pyper & Adelman (2017) determined a photometric period of 7850 d. M17 adopted the 7936.522 day period, indicating an incomplete phase coverage. This author always observed well split FeII 6149.258 Å Zeeman components, consistent with $B_s > 4000$ G, an exception (unsplit line) occurring on JD = 2450 797.312.

We have observed HD 9996 between 2001 and 2021, in addition we have retrieved 2 GECKO spectra from the CFHT archive, one of those obtained in 2000. Our B_s measurements of HD 9996 are listed in Table 8. We find that the variability period given by P17 is representative of the B_s and B_e variations of HD 9996 (Figure 4) with a well-defined maximum and a rather flat minimum. This is not rare for this class of stars (see HD 318107 or HD 335238 later in the text), although in the case of HD 9996 it could be that the observed plateau is a consequence of the difficulty in measuring such weak B_s fields because of the merging of the Zeeman subcomponents of the FeII 6149.258 Å line (see Figure 4). Near-infrared lines – more sensitive because of the λ^2 dependence of Zeeman-splitting

– should preferably be used to determine the real minimum in the B_s variations of HD 9996. Leone et al. (2003) have shown an application of this technique to magnetic stars by selecting suitable spectral lines with large effective Landé factors (Solanki 1994).

Figure 4 also shows some of these spectra ordered with time; it confirms the finding by Preston & Wolff (1970) that the respective equivalent widths of chromium and rare-earth spectral lines change out of phase. The B_s maximum coincides with the negative extremum of B_e , while from phases 0.3 through 0.7 B_e presents a maximum, B_s staying constant at its minimum value. If the flat minimum is real, HD 9996 presents a magnetic field that is not purely dipolar. With a value $q = B_s^{\max}/B_s^{\min} \geq 3$, HD 9996 appears a rather extreme MCP star, since there is no other known case with q larger than 2 (see figure 2 in M17).

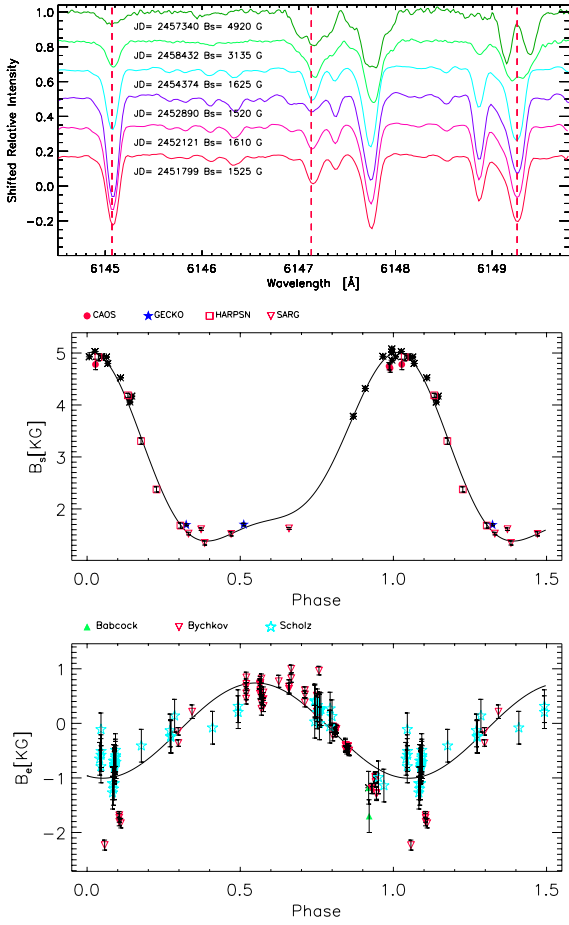


Figure 4. HD 9996. Top, chunks of spectra with the FeII 6149.258 Å, CrII 6147.154 Å and NdIII 6145.070 Å lines marked. The normalised spectra are shifted vertically and ordered with decreasing values of B_s . Cr (λ 6147) and Nd (λ 6145) abundances change out of phase. Central and lower panels show the B_s and B_e variations folded with the 7850 d period. Errorbars (tens of G) for B_s measurements are smaller than symbols and are barely visible.

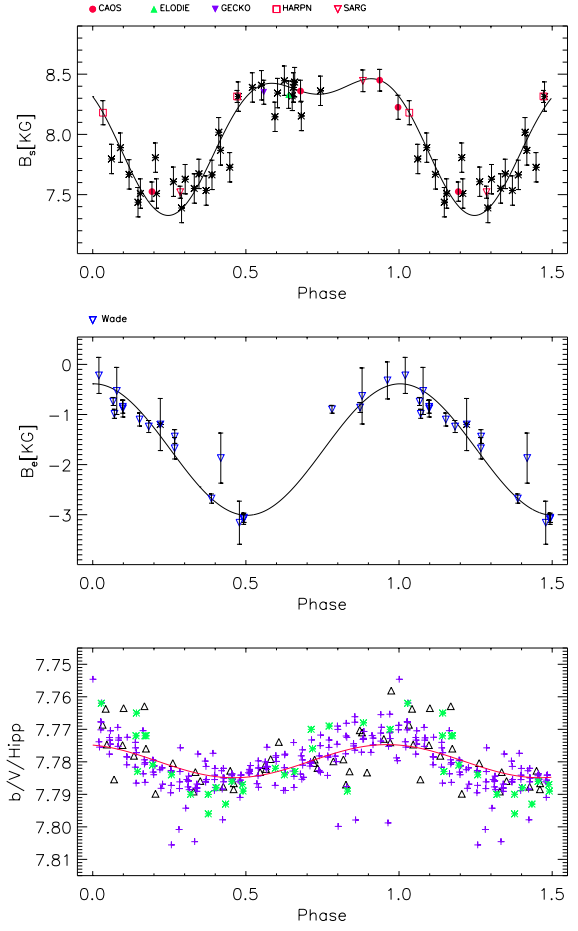


Figure 5. HD 12288

Figure 6. HD 12288. Variability in B_s , B_e , and photometry – Wolff & Morison (1973) (*), HIPPARCOS (Δ) and MASCARA (+) – folded with the 34.993 d period.

3.4 HD 12288

Bernhard et al. (2020) established HD 12288 as a photometric variable with the ephemeris $JD(V^{\max}) = 2457\,218.6 + 35.73 \pm 0.03$ d, presenting a peak-to-peak difference of 0.02 mag. According to P17, this star is variable in the Strömgren u , v and b filters with a 34.99 d period, but it presents a constant Strömgren y magnitude. A period of 34.9 d was adopted by M17 to discuss the magnetic variability of HD 12288.

We have observed HD 12288 eight times and obtained 1 spectrum from the ELODIE archive and 1 from the CFHT archive. In accord with P17, we found the TESS (600–1000 nm) magnitudes obtained between 2458 790 and 2458 841 to be constant (7.63688 ± 0.00006). A Lomb-Scargle analysis of our measurements (Table 9), together with the M97 and M17 B_s data, the Wade et al. (2000b) B_e values, and photometry by Wolff & Morrison (1973), MASCARA (Talens et al. 2017; Bernhard et al. 2020), and HIPPARCOS (van Leeuwen 2007) leads to a period of 34.993 ± 0.003 d, corresponding to the highest peak of $LS(B_s, B_e, Mag.)$. The data folded with this period are shown in Fig. 6. It would seem that HD 12288 is presenting some quite singular behaviour among the MCP stars: B_s remains almost constant (at the maximum value of 8.5 kG) during half of the rotation period, at the same time B_e goes from -3 kG to near zero. The decrease of B_s to about 7.5 kG is accompanied by a change in B_e down again towards -3 kG. This star becomes brighter as B_e weakens.

3.5 HD 14437

The variability period of HD 14437 was determined to 26.87 ± 0.02 d by Wade et al. (2000b) from B_e measurements. From MASCARA data, Bernhard et al. (2020) found a photometric period of 26.78 ± 0.01 d. Measurements of B_s by M97 and M17 cover the years from 1991 to 1997, our 11 spectra were obtained between 2001 and 2021. We have performed a Lomb-Scargle analysis of our data (Table 10) together with the M97 and M17 B_s measurements, the Wade et al. (2000b) B_e values, and the photometry by HIPPARCOS, TESS, and MASCARA. The period that best reproduces all these variations is 26.734 ± 0.007 d (Fig. 7).

3.6 HD 18078

From B_s and B_e measurements, the variability period of HD 18078 has been determined by Mathys et al. (2016b) to 1358 ± 12 d. We have obtained 10 high-resolution spectra of HD 18078 from 2003 up to 2021 with SARG, CAOS, and HARPS-North, and retrieved spectra from the CFHT and Elodie archives. When the period given by Mathys et al. (2016b) is adopted, our B_s measurements (Table 11) are slightly in advance. A simultaneous Lomb-Scargle analysis of our B_s measurements, Mathys et al. (2016b) B_s and B_e data, and HIPPARCOS and Strömgren y photometry (Mathys et al. 2016b) yields $LS(B_s, B_e, Mag.)$ with the main peak at 1352 ± 6 d. B_s and B_e data, together with HIPPARCOS and Strömgren y photometry (Mathys et al. 2016b) are shown in Fig. 8.

3.7 HD 29578

From spectra collected between $JD = 2449\,298$ and $2451\,084$ (~ 1786 days), M17 found that the surface magnetic field of HD 29578 changes with a period much longer than 1800 days. We have obtained one spectrum of HD 29578 with UCLES at the AAT on $JD = 2457\,056.992$, but unfortunately the FeII 6149.258 Å line

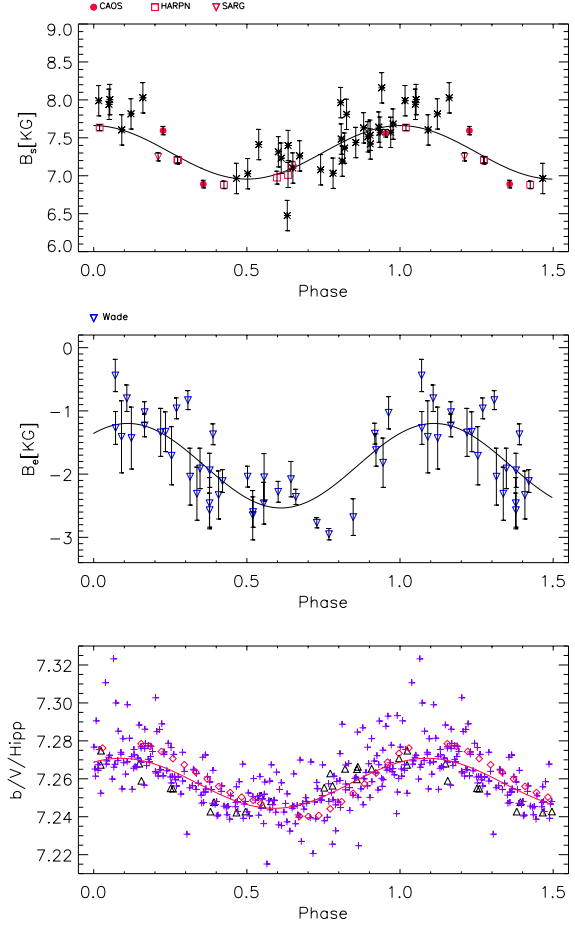


Figure 7. HD 14437. Variability in B_s , B_e , and photometry – HIPPARCOS (Δ), TESS (\diamond), MASCARA (+) – folded with the 26.734 d period.

region was not included. From other lines the surface magnetic field was estimated at ~ 2900 G. We have also obtained 1 UVES and 2 FEROS spectra from the ESO archive. These B_s measurements (Table 12), plus the ones by M97, M17 and Ryabchikova et al. (2004) extend the time-frame of magnetic measurements to 7759 days.

We have performed a Lomb-Scargle analysis of all available B_s measurements, finding two comparable peaks at 4000 and 9370 days in the periodogram (Table 3). Fig. 9 shows the B_s and the B_e (M17) measurements, folded with both periods respectively. It appears that new measurements are necessary to reliably determine the period of HD 29578. Fig. 10 shows the variation of the HD 29578 spectrum over time, from $JD = 2451\,946$ (when Zeeman subcomponents are clearly visible) to $2457\,056$, when these overlap. NIR high-resolution spectroscopy is desirable in order to define the B_s variability of HD 29578.

3.8 HD 47103

From B_s measurements, obtained between $JD = 2449\,816$ and $2451\,085$, M17 found HD 47103 to be variable with an extremely long period. Our measurements of B_s (Table 13) extend the time baseline to 7600 days. We have computed the Lomb-Scargle periodogram $LS(B_s)$ of our B_s measurements in combination with those taken from the literature (Babel & North 1997; Mathys 2017), and the Lomb-Scargle periodogram of the B_e measurements by Elkin

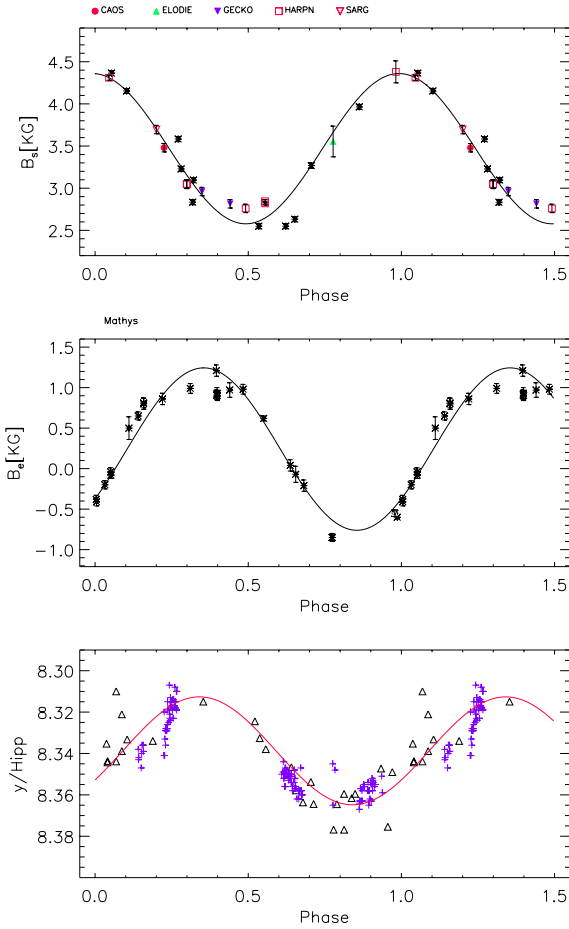


Figure 8. HD 18078. Variability in B_s , B_e (Mathys et al. 2016b), and photometry – HIPPARCOS (\triangle), Mathys et al. (2016b) (+) – folded with the 1352 d period. Errorbars for the B_s measurements are barely visible, being often smaller than symbol size.

& Wade (1997) and M17. $LS(B_s, B_e)$ peaks at 17.683 ± 0.004 d. Fig. 11 presents the variability in B_s and B_e .

3.9 HD 50169

Mathys et al. (2019a) found the B_e variability period of HD 50169 to be 10600 ± 300 d. This value is also representative of their measurements of the surface magnetic field, which however cover only 9856 days, an interval shorter than a full rotation cycle. Our B_s measurements (Table 14) slightly extend the time-frame to 10109 days. These data confirm the period advanced by Mathys et al. (2019a) and establish the shape of the minimum of the variations in B_s . The uncertainty in the period of 300 days is due to the B_e measurements, it cannot be made smaller here. The data are folded in Fig. 12 with the ephemeris given in Table 3.

3.10 HD 51684

From 10 measurements of B_s collected between JD = 2 450 162 and 2 451 086, M17 concluded that the variability period of HD 51684 is 371 ± 6 d. In the ESO archive, we found 5 additional UVES spectra spread over 330 days. A Lomb-Scargle analysis of our measurements (Table 15) together with those of Mathys gives a slightly

shorter variability period: 366 ± 1 d. Data folded with this period are shown in Fig. 13.

3.11 HD 55719

M17 analysed B_s measurements, collected from JD = 2 447 285 to 2 451 086, and found the rotational period of HD 55719 to be much longer than 10 years. Our measurements of B_s (Table 16) and those from the literature cover more than 10000 days. We note that the surface magnetic field of HD 55719 has always been decreasing over the last 27 years, with a resulting rotation period not shorter than 14000 days (38 years) by assuming a simple sinusoidal variation (Fig. 14).

3.12 HD 61468

M17 found B_s in HD 61468 to be variable with a 322 ± 3 d period. We have obtained a spectrum of this star with HARPS-North on JD = 2 457 340.717 and measured a value of $B_s = 6260 \pm 85$ G. A Lomb-Scargle periodogram of the combined B_s values presents 2 merged peaks centred at 321 and 325.5 d. A sine fit to the data favours a variability period equal to 321 ± 1 d. Fig. 15 shows the periodic variability of the surface field of HD 61468 with the ephemeris given in Table 3.

3.13 HD 75445

M17 found HD 75445 to be variable in B_s with a small amplitude and a period of 6.291 d. Our measurements (Table 18), combined with the surface magnetic field values from M17 and Ryabchikova et al. (2004), span the interval from JD = 2 449 457 to 2 454 205 (~ 13 yr) and reveal an average value of $\langle B_s \rangle = 2936 \pm 49$ G. A Lomb-Scargle analysis results in a large number of peaks of similar importance, with the highest three at 2.5026, 3.2926 and 6.5500 d.

The constant magnitude (6.9000 ± 0.0003) measured with TESS over 50 days (JD = 2 458 517 - 2 458 568), together with the B_s r.m.s. error (comparable to the measurement uncertainty) suggests that the period of variability – provided there is any – of HD 75445 must be considerably longer than 13 years (Fig. 16).

3.14 HD 81009

From B_s and B_e measurements, Wade et al. (2000c) determined the variability period of HD 81009 to 33.984 ± 0.055 d. P17 concluded that the photometric variability period of this star is 33.987 ± 0.002 d. Our B_s measurements (Table 19) extend the time coverage of B_s from 1954 to 8210 days. A Lomb-Scargle analysis of the B_s data confirms the period found by P17. Fig. 17 shows the periodic variability of HD 81009 in B_s .

3.15 HD 93507

The period of the variability of HD 93507 in B_s and B_e is 556 ± 22 d (M17). We have obtained from the ESO archive 1 UVES and 31 HARPS spectra. A Lomb-Scargle analysis of B_s measurements by M17, our results (Table 20) and B_e measurements by Mathys (2017) yields a variability period of 562 ± 5 d (Fig. 18).

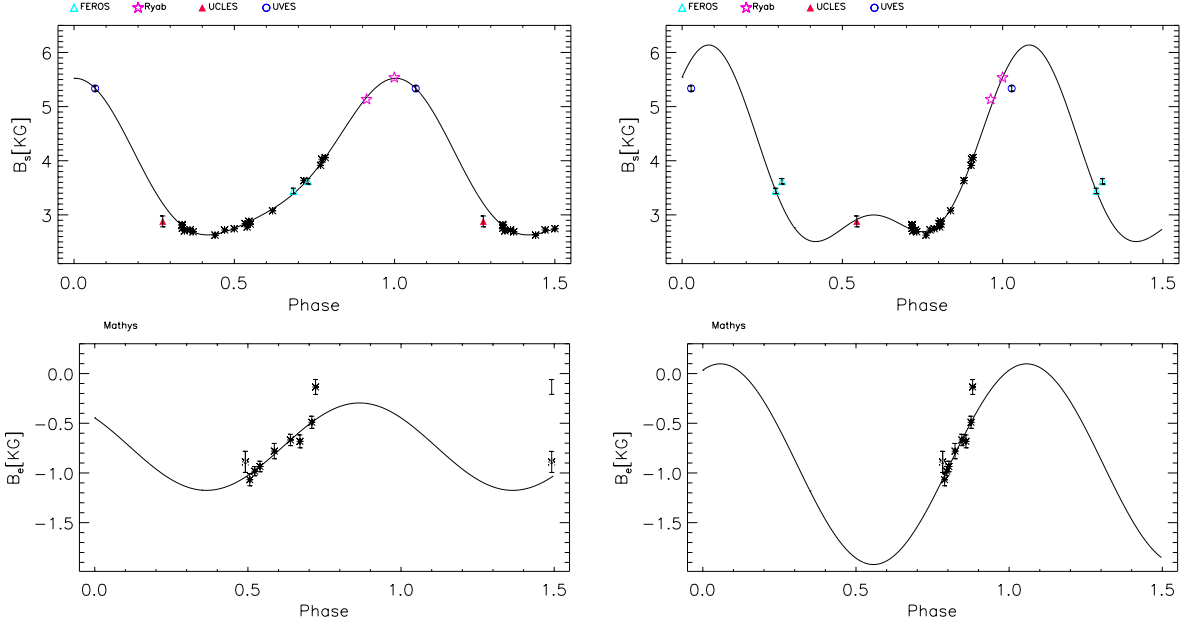


Figure 9. HD 29578. Variability of B_s and B_e . In the left panels the data are folded with the 4000 day period, in the right panels with the 9370 day period. A sinusoidal fit to the B_e data helps to visualise the possible variability. Errorbars for the B_s measurements are barely visible, being often smaller than symbol size.

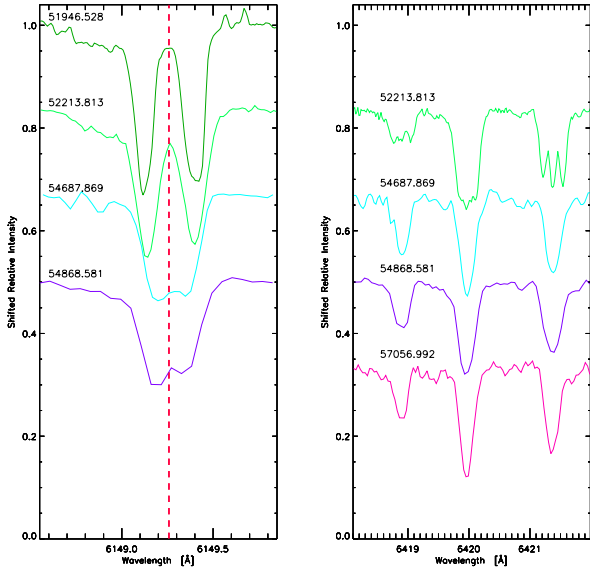


Figure 10. HD 29578. Chunks of spectra ordered with decreasing B_s ; x-axis values correspond to JD - 2 400 000. The CES@3.6m-ESO spectrum (JD = 2 451 946.528) extends from 6120 to 6150 Å. The UCLES@AAT spectrum (JD = 2 457 056.992) does not include the FeII 6149.258 Å line; Zeeman splitting of other metal lines is indicative of a surface magnetic field of about 2900 G.

3.16 HD 94660

Hensberge (1993) discovered HD 94660 to be photometrically variable with a period close to 2700 days. From spectra acquired on 12 different nights between May 2001 and April 2014, Bailey et al. (2015) found that this star belongs to a binary system with an orbital period of 840 d and they adopted the rotational period ($P = 2800 \pm 250$ d) determined by Landstreet et al. (2014). A similar

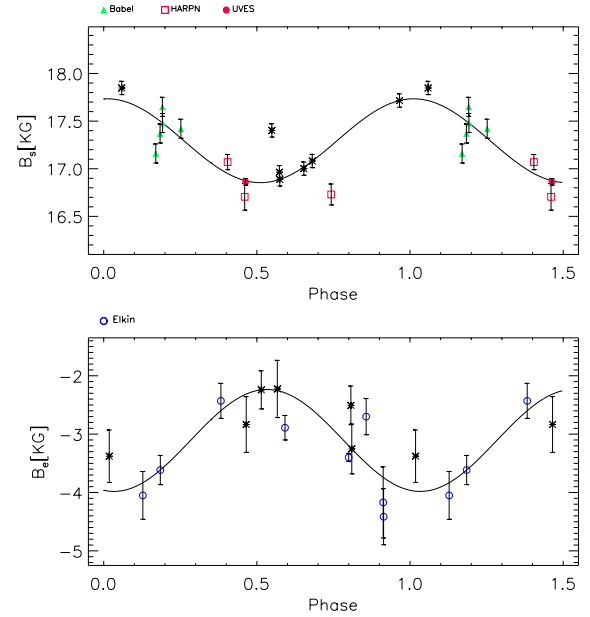


Figure 11. HD 47103. B_s and B_e variability, folded with the 17.683 d period. Circles denote data from Elkin & Wade (1997).

value ($P = 2800 \pm 200$ d) was determined independently by M17 from B_s measurements. We have retrieved the ESO and CFHT archive spectra published by Bailey et al. (2015) and 11 high-resolution spectra were obtained between January 1998 and December 2009 with UCLES at the AAT. The Lomb-Scargle periodogram of our (Table 21), M97 and M17 B_s measurements $LS(B_s)$ peaks at 2830 ± 140 d. Fig. 19 presents the periodic variability in B_s of HD 94660.

Radial velocities measured (Table 5) in the UCLES spectra of HD 94660 are combined with the values given by Bailey et al.

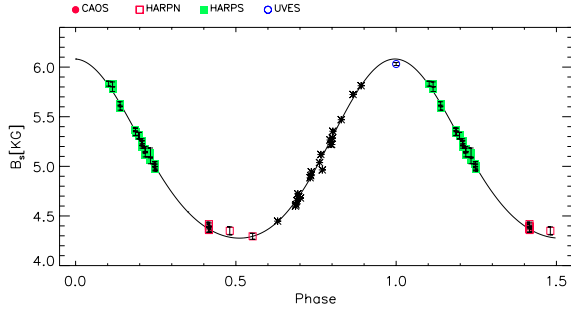


Figure 12. HD 50169. B_s variability, folded with the 10600 d period.

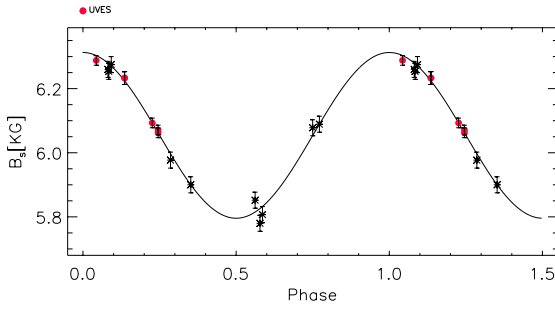


Figure 13. HD 51684. B_s variability, folded with the 366 d period.

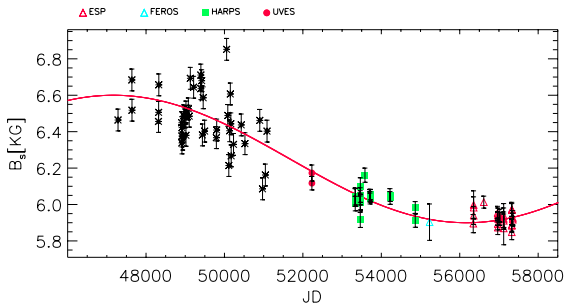


Figure 14. HD 55719. B_s over time. The sine fit to the data is based on the shortest possible period of 14000 d.

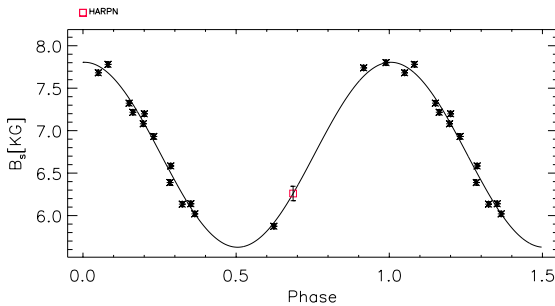


Figure 15. HD 61468. B_s variability, folded with the 321 d period. Errorbars (tenths of G) for B_s measurements can be smaller than symbols and barely visible.

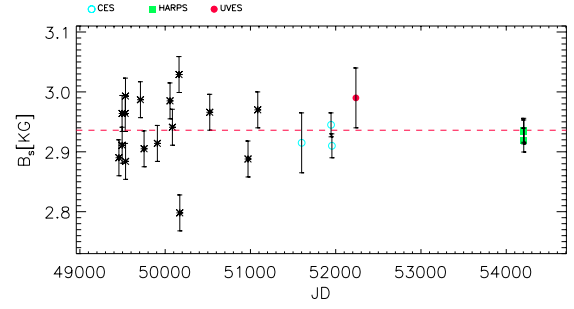


Figure 16. HD 75445. B_s over time. A straight line equal to the average value of the surface field is also plotted.

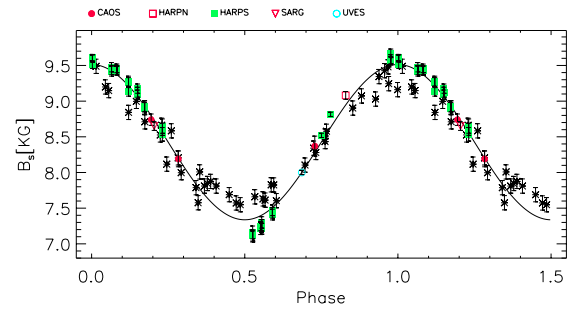


Figure 17. HD 81009. B_s variability, folded with the 33.987 d period.

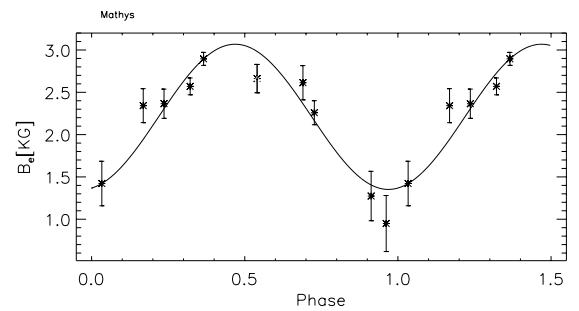
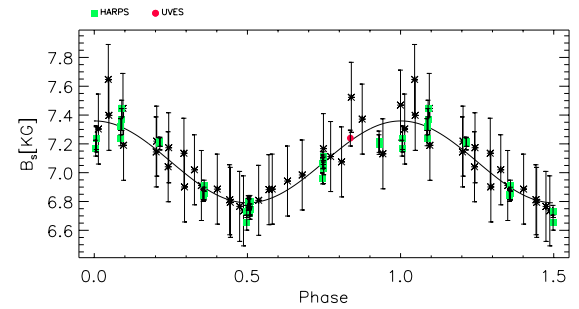


Figure 18. HD 93507. B_s and B_e variability, folded with the 562 d period.

(2015) and M17 to determine the orbital parameters, following Catanzaro et al. (2016). We found the orbital period $P_{\text{Orb.}} = 848.96 \pm 0.17$ d, periastron passage epoch $T_0 = 2445627.9 \pm 2.1$, eccentricity $e = 0.445 \pm 0.006$, angular anomaly $\omega = 264.1 \pm 0.9$ degrees, amplitude of radial velocity variation $K = 17.86 \pm 0.13$ km s⁻¹ and system velocity $\gamma = 18.52 \pm 0.08$ km s⁻¹. Radial velocities of HD 94660 folded with the here found orbital period are plotted in Fig. 19. Errors in the orbital parameters are computed as the difference in the parameter resulting in an incre-

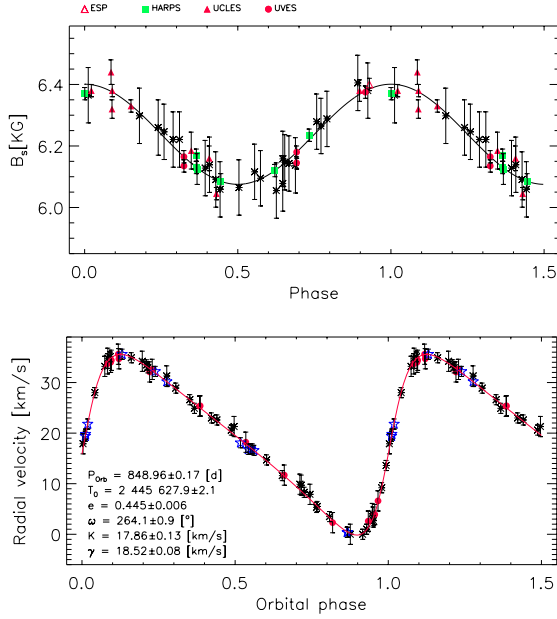


Figure 19. HD 94660. Top panel, B_s variability folded with the 2830 d period. Bottom panel, our radial velocities measured in the UCLES spectra (filled circles) with Bailey et al. (2015) (stars) and M17 (*) values. Continuous line is the orbital solution fitting at the best the observations.

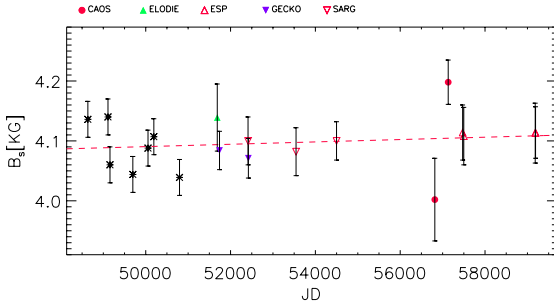


Figure 20. HD 110066. B_s over time. A linear fit suggests constant behaviour.

ment of the χ^2 equal to 1. Within errors, these are in agreement with the M17 results.

Because of the X-ray emission from the HD 94660 binary system, the nature of the companion is still a matter of debate (Oskina et al. 2020; Schöller et al. 2020).

3.17 HD 110066

Pyper & Adelman (2017) reported on a 12-year photometric campaign dedicated to HD 110066, finding no evidence of variability. M17 noted that the B_s variability of this star presents an amplitude of 100 G if the period is as long as 4900 days. Bychkov et al. (2021) have obtained new B_e measurements and – discarding the results published by Babcock (1958) – established a variability period of 6.4769 days. We have analysed TESS photometric data and found a constant magnitude (6.346238 ± 0.000003) between JD=2 458 900.0 and 2 458 926.5 (26 days).

We have obtained high-resolution spectra of HD 110066 with SARG and CAOS and have retrieved spectra from the Elodie, CFHT and ESO archives. Our B_s measurements of HD 110066 are

Table 5. Radial velocities (RV) of HD 94660 from archive UCLES spectra. Errors are of 1 km s^{-1} order.

HJD 2400000+	RV km s^{-1}	HJD 2400000+	RV km s^{-1}
48968.261	1.6	52980.254	11.7
49350.250	25.3	53369.254	35.6
49351.258	25.4	54188.098	33.7
50060.244	32.5	54196.964	34.0
50824.041	35.6	54198.928	34.4
51176.136	18.2	54928.960	3.9
51542.171	6.6	55161.232	32.6
52265.250	2.3		

listed in Table 22. Including values from M97 and M17, we span a period of 28.8 years without detecting any variability. All B_s measurements range between 4040 and 4150 G, with errors not smaller than 50 G. On the basis of B_s measurements, we can only conclude that the variability period – provided there is any – of HD 110066 exceeds 3 decades, see Fig. 20.

3.18 HD 116114

From measurements collected between JD = 2 448 732 and 2 451 042, M17 found HD 116114 to be a magnetic variable with a 27.61 ± 0.08 d period. The amplitude of the B_s variations is 33 ± 9 G, the amplitude of the B_e variations is 84 ± 33 G. M17 ruled out the 4.4156 d period determined by Romanyuk et al. (2014) from B_e measurements. Wraight et al. (2012) concluded that HD 116114 is a photometric variable with a period of 5.3832 d.

We have analysed the TESS data of HD 116114 (between JD = 2 458 570 and 2 458 595), finding a constant magnitude (6.76799 ± 0.00001) on a time scale of 25 days. We have observed HD 116114 with SARG, HARPS, CAOS, UCLES and HARPS-North. In addition, we have retrieved NTT, UVES and HARPS spectra from ESO archive. Our B_s measurements are listed in Table 23. The B_s measurements cover 8855 days, revealing a steadily increasing field. Assuming sinusoidal variations, the shortest possible period of HD 116114 would therefore be of the order of 48 years (Fig. 21). The B_e measurements by Mathys & Hubrig (1997), Romanyuk et al. (2014), and Mathys (2017) on the other hand do not present a clear trend (Fig. 21).

3.19 HD 126515

Leone & Catanzaro (2001) noted the coincidence of the extrema of literature light curves of the star HD 126515 when a variability period of 129.9474 d is assumed. This period turned also out to be representative of the B_e and B_s variations. P17 and M17 established a period of 129.95 ± 0.02 d from photometric and magnetic data. By adding our B_s measurements (Table 24) to the data published by Preston (1970), M97 and M17, we span a total of 23250 days. A Lomb-Scargle analysis of these measurements confirms the validity of the 129.95 d period. Fig. 22 shows the respective variations in B_s and in B_e , based on measurements by Babcock (1958), van den Heuvel (1971), Mathys et al. (1997), Wade et al. (2000a), Leone & Catanzaro (2001), and Mathys (2017).

The B_s maximum coincides with the negative B_e extremum, while the B_s minimum is found close in phase with zero effective field B_e . This constitutes clear evidence for a non-axisymmetric

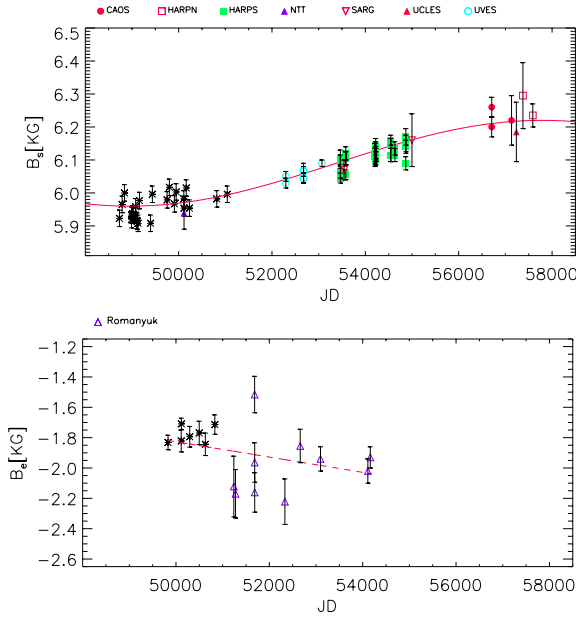


Figure 21. HD 116114. B_s and B_e variations over time. A sine fit with the shortest possible period of 17700 d is plotted over the B_s measurements. The B_e measurements have been linearly fitted.

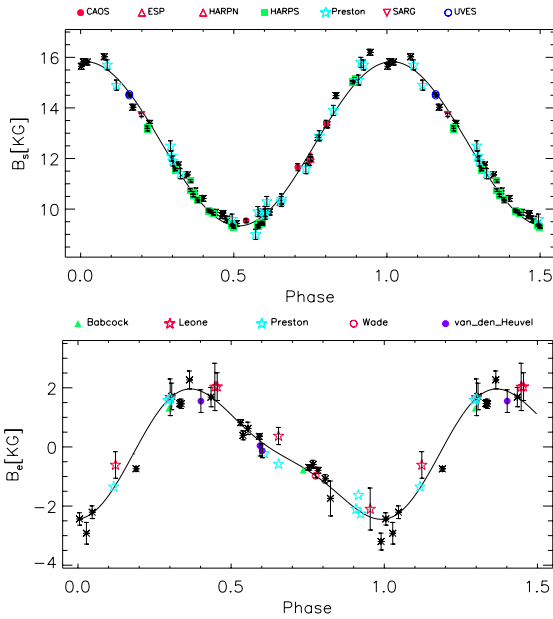


Figure 22. HD 126515. B_s and B_e variability, folded with the 129.95 d period.

magnetic field geometry of HD 126515 (Stift 1975; Stift & Goossens 1991).

3.20 HD 137949

After 14 years of monitoring, no evidence of photometric variability has been detected by P17. Referring to B_e measurements spanning almost 50 years, Landstreet et al. (2014) estimated the rotational period of this star to be of the order of one hundred years, M17 concluded on a variability period probably of the order 5195

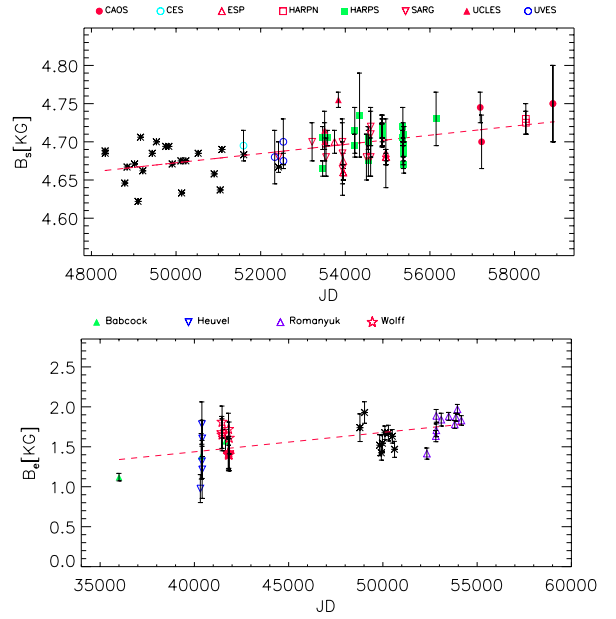


Figure 23. HD 137949. B_s and B_e measurements over time. The straight lines represent linear fits to the data.

days (~ 14.2 yr). By combining our measurements (Table 25) with data available in the literature, we cover 10584 days, corresponding to twice the period put forward by Mathys and coworkers. A Lomb-Scargle analysis of B_s and B_e data does not show any predominant peak in the periodogram. Fig. 23 displays B_s and B_e over time. The trends seen in both plots are not incompatible with a slight increment in field strengths; if real, this would indicate a rotational period much longer than 27 years.

Even if all spectra of HD 137949 recorded between 2002 and 2018 appear constant, with equally strong red and blue σ components for all species, in the SARG spectra obtained on 2006 July 13, 14 and 15 the blue σ components appear much weaker than the red ones. This difference is particularly large for chromium lines, only marginal for iron lines. We have no idea how persistent and recurrent this phenomenon might turn out; we can only state that it started later than 2006 April 10, and that it ended before 2006 August 1 (Fig. 24). Contemporaneous observations of other stars, e.g. HD 216018 also presented in this paper, rule out any technical problems that would result in spurious spectral line profiles. We are not aware of a similar spectral line change observed before in a magnetic chemically peculiar star.

3.21 HD 142070

From Strömgren photometry, Adelman (2001) established HD 142070 as a photometric periodic variable with the largest amplitude in the v filter and the ephemeris: $\text{HJD}(v^{\min}) = 2\,450\,837.499 + 3.37189 \pm 0.00007$ E. M17 found this star to be also magnetically variable with a period of 3.3718 ± 0.0011 d.

We have obtained 4 new spectra of this star with CAOS, UVES and HARPS-North, in addition we have retrieved 2 UVES and 35 HARPS spectra from ESO archive. Our measurements of B_s are listed in (Table 26). The product $LS(B_s, B_e, v)$ of the periodograms of all available B_s measurements, of B_e data from M17 and Romanyuk et al. (2014), and of Strömgren v photometry (Adelman 2001) peaks at 3.3721 ± 0.0002 d. Fig. 25 shows the double wave

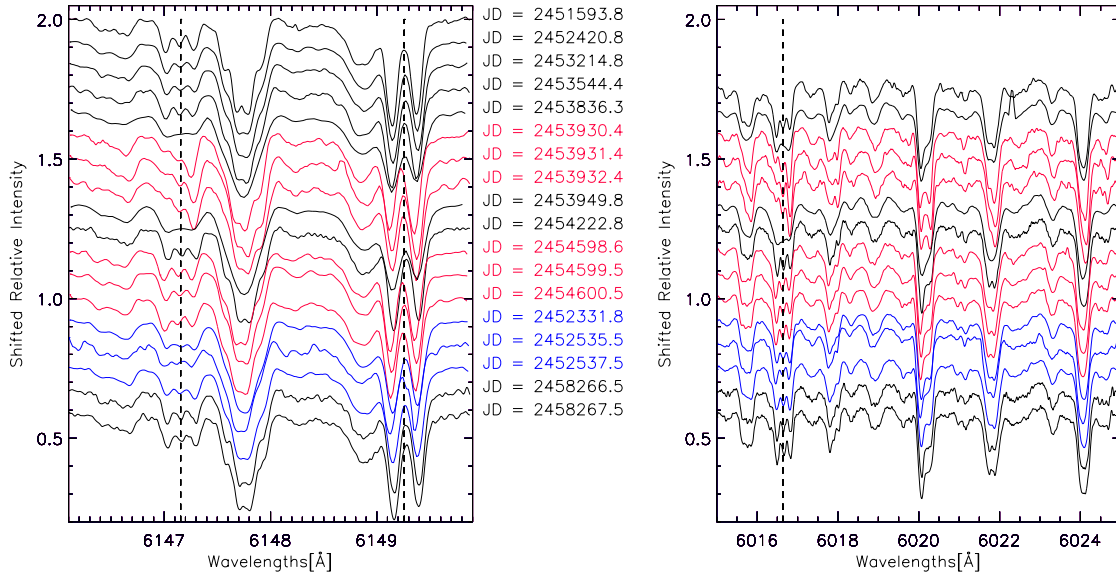


Figure 24. HD 137949. On three consecutive nights, from JD = 2453930 to 2453932 (2006 July 13, 14, and 15) SARG spectra presented red σ Zeeman subcomponents deeper than the blue ones, especially in chromium lines. Other series of observations on consecutive days did not exhibit similar behaviour. ESPaDOs spectra obtained on JD = 2453836 and 2453949 do not show clearly separated Zeeman subcomponents because of the reduced resolution as compared to other spectrographs, they however reveal that the phenomenon did not last longer than 110 days.

variation of B_s whose extrema coincide in phase with the B_e maxima, based on the ephemeris given in Table 3.

3.22 HD 144897

The variability period of the surface magnetic field of HD 144897 was determined by M17 to 48.57 ± 0.15 d from data collected over 7.1 years.

We have obtained 1 spectrum of HD 144897 with UCLES and retrieved 1 UVES spectrum and 28 HARPS spectra from the ESO archive. M17 and our values of B_s (Table 27) cover a total range of 22.5 years. A Lomb-Scargle analysis gives 48.60 ± 0.02 d. Fig. 26 shows all available measurements of B_s and B_e (Mathys 2017), phased with the ephemeris given in Table 3. Both variations are fairly sinusoidal and the B_s minimum in coincidence with the B_e maximum is proof of a magnetic field geometry far from a centred dipole configuration.

3.23 HD 150562

B_s measurements of HD 150562 have been published by M97 and M17, spanning an interval of 4.5 years, Mathys and coworkers concluded that the variability period of this star exceeds 4.5 years.

We have observed this chemically peculiar star once with UCLES, and we have obtained from ESO archive 1 EMMI, 1 UVES and 11 HARPS spectra. With our B_s values (Table 28), the coverage now extends over 21.3 years. Lomb-Scargle analysis of our and Mathys' measurements produces a periodogram with the highest peak at 2100 days. Fig. 27 shows the B_s data folded with this period. Measurements of B_e by Bagnulo et al. (2015) and M17, plotted in the same figure, are too scanty to draw conclusions as to the variability.

At the phase of the maximum, we find an "unexpected" B_s value obtained on JD = 2450171.802 that M17 ascribed to an

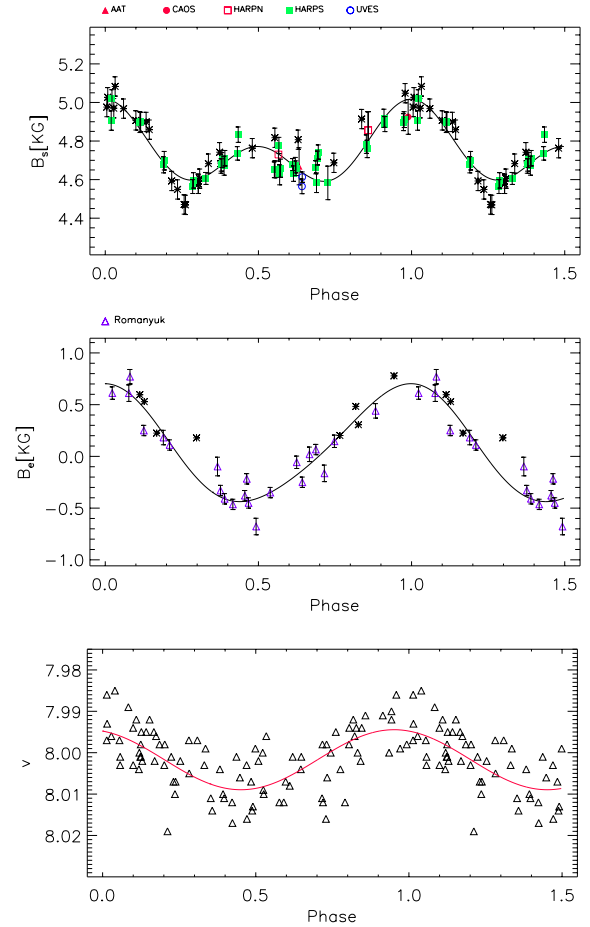


Figure 25. HD 142070. B_s , B_e and Strömgren v magnitude variations, folded with the 3.3721 d period.

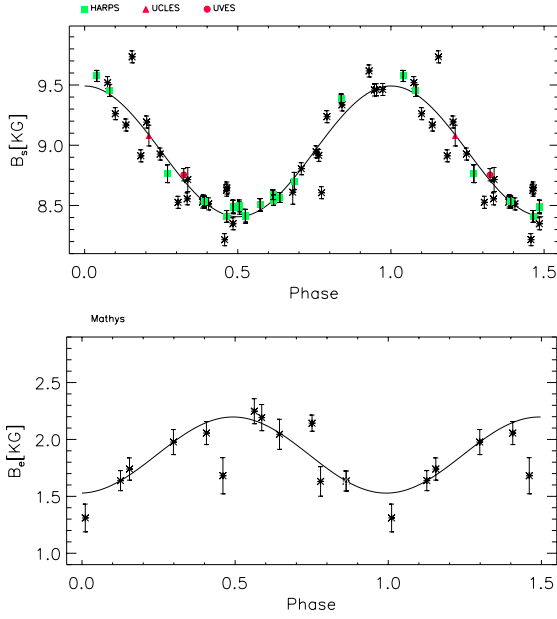


Figure 26. HD 144897. B_s and B_e variability, folded with the 48.60 d period.

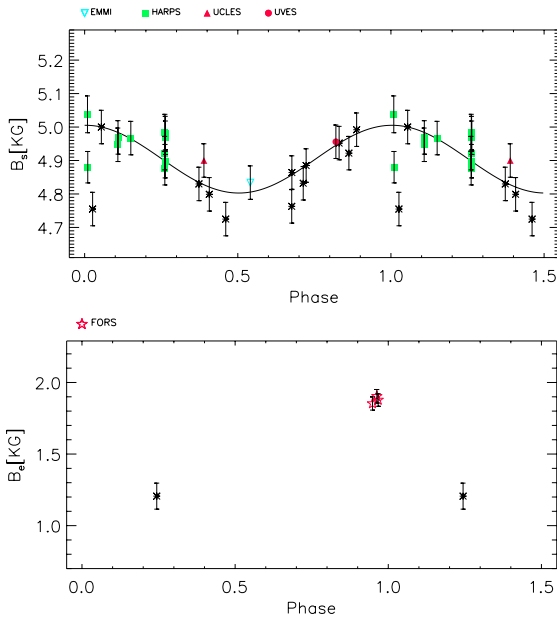


Figure 27. HD 150562. B_s and B_e variability, folded with the 2100 d period. B_e measurements with FORS are from [Bagnulo et al. \(2015\)](#).

unidentified cosmic ray. At the same phase, we find another “unexpected” value measured in a HARPS spectrum acquired on JD = 2454 338.582. HD 150562 should be observed in 2024 during the next B_s maximum to check if this is the result of chance or if some physical reason can be identified (e.g. partial occultation of the visible stellar disk by a secondary star).

3.24 HD 154708

The Zeeman subcomponents of the FeII 6149.258 Å line of HD 154708 are distant by $\Delta\lambda > 1$ Å, implying that in the linear Zeeman approximation the field is about 24000 G, one of the strongest

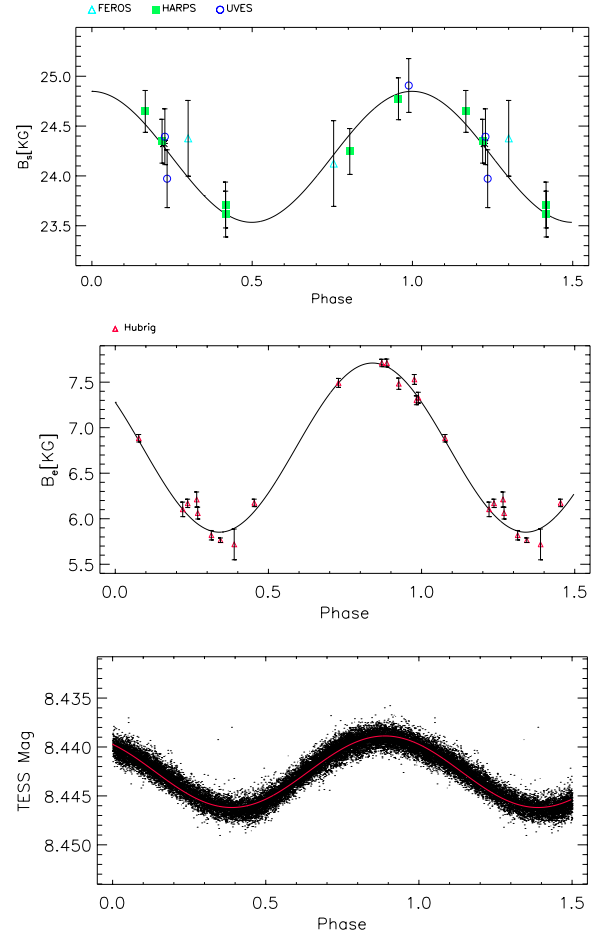


Figure 28. HD 154708. Variability in B_s , B_e , and TESS photometry, folded with the 5.367 d period. B_e measurements by [Hubrig et al. \(2009\)](#) are based on hydrogen lines.

known fields for a non degenerate star ([Hubrig et al. 2005](#)). From B_e measurements, the variability period of HD 154708 has been determined by [Hubrig et al. \(2009\)](#) to 5.3666 ± 0.0007 d, whereas [Landstreet et al. \(2014\)](#) arrived at 5.363 ± 0.003 d. A geometrical model of the magnetic field of HD 154708 has been published by [Stift et al. \(2013\)](#).

We have obtained 4 UVES, 6 HARPS and 2 FEROS spectra of HD 154708 from ESO archive. Our $\Delta\lambda$ measurements have been converted to B_s values (Table 29) with the help of eq. 1. This means that we are neglecting the partial Paschen-Back effect is expected to play a role on account of the strong magnetic field (see [Stift et al. 2008](#)). The resulting B_s values will thus constitute lower limits to the actual surface magnetic field, but they remain still representative of its variability. Including in the Lomb-Scargle analysis the B_e values published by [Hubrig et al. \(2009\)](#) and TESS magnitudes, the highest peak of the product $LS(B_s, B_e, TESS)$ occurs at 5.367 ± 0.001 d. Fig. 28 shows the variability in B_s , B_e , and TESS photometry, based on the ephemeris given in Table 3. It appears that light variability is driven by the longitudinal component of the field, while the B_s variations are shifted in phase by 0.15.

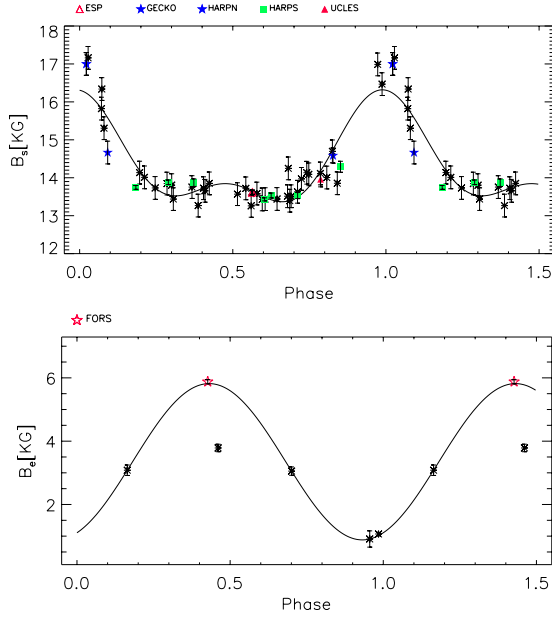


Figure 29. HD 318107. Variations in B_s and B_e folded with the 9.7089 d period.

3.25 HDE 318107

The B_s and B_e variability period of 9.7088 ± 0.0007 d was determined by Bailey et al. (2011). We have obtained 7 HARPS spectra from the ESO archive, 1 GECKO spectrum, and 2 ESPaDOns spectra from the CFHT archive. In addition, we have obtained 1 new spectrum with UCLES and 2 spectra with HARPS-North. Our 13 B_s measurements (Table 30) have been combined with values from M17 for a Lamb-Scargle analysis that peaks at 9.7089 ± 0.0002 days. Fig. 29 shows the periodic variability in B_s and B_e (Mathys & Hubrig (1997), Bagnulo et al. (2015), M17) of HDE 318107.

3.26 HD 165474

M97 and M17 presented B_s measurements of HD 165474 obtained between 1989 (JD=2 447 642) and 1998 (JD=2 450 972), leading to the conclusion that the field is continuously increasing and that the variability period largely exceeds 9 years. On the other hand, our B_s measurements between 2004 (JD=2 453 104) and 2015 (JD=2 457 229) are steadily decreasing, with evidence of a new increase in the HARPS-North data obtained in 2018 and 2021 (Table 31). Including B_s measurements from Preston (1971) and Nielsen & Wahlgren (2002), under the hypothesis of a single harmonic variation, the period can be no shorter than 9900 days (27.1 yr): Fig. 30. The scarcity of B_e (Babcock 1958; Mathys 1994; Mathys et al. 1997; Romanyuk et al. 2014) data does not allow any definite conclusions.

3.27 HD 166473

The B_s variability of HD 166473 has very recently been analysed by Mathys et al. (2020), using spectra collected from ESO and ESPaDOns archives. These authors determined a period of 3836 days. We too have obtained HD 166473 spectra from the ESO and CFHT archives and added 1 new measurement: $B_s = 7210 \pm 65$ G, obtained by us with UCLES at the Anglo Australian Telescope on

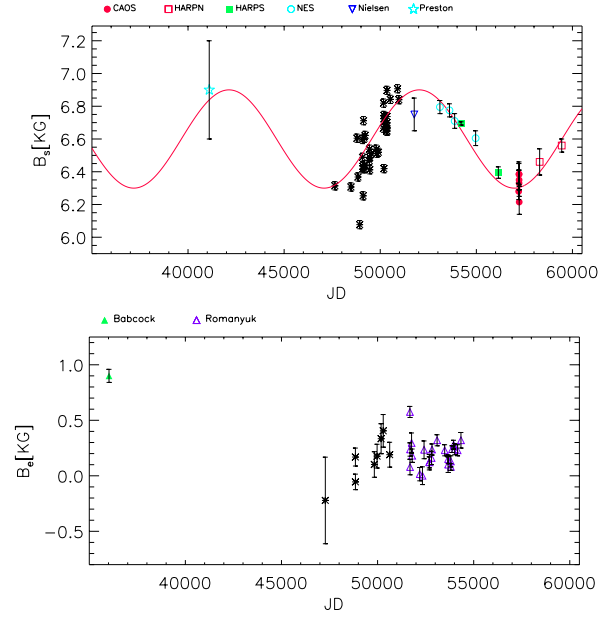


Figure 30. HD 165474. B_s and B_e measurements over time. It appears that the shortest possible period for the B_s variability is 9900 days.

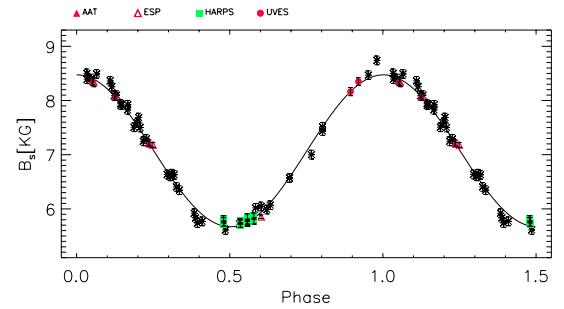


Figure 31. HD 166473. B_s variability, folded with the 3836 d period.

JD = 2 457 235.008. Our measurements (Table 32) confirm the published period, and Fig. 31 shows the B_s variability, folded with the ephemeris determined by Mathys and coworkers (Table 3).

3.28 HD 177765

Eight measurements of B_s distributed from 1993 to 1998, plus one measurement taken from the literature and obtained in 2010, led M17 to the conclusion that the variability period of HD 177765 exceeds 17 years. We have recovered 1 FEROS spectrum and 1 UVES spectrum from the ESO archive and observed HD 177765 once with UCLES, 2 times with HARPS-North. Our B_s measurements (Table 33) extend the temporal baseline from 6 years to almost 25 years and reveal a continuous increase with time. Under the assumption of a simple harmonic variation, we estimate the shortest possible period at 37 years (Fig. 32).

3.29 HD 178892

From B_e measurements and HIPPARCOS photometry, Semenko et al. (2011) determined the variability period of HD 178892 to

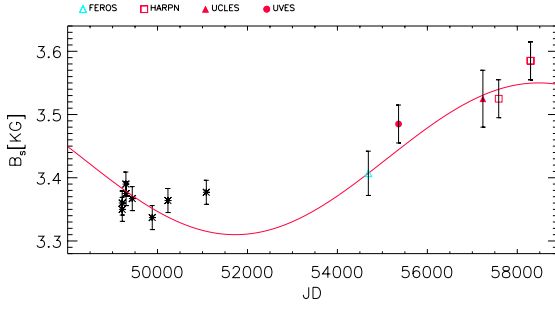


Figure 32. HD 177765. B_s measurements over time. A sine fit to the data with the shortest possible period of 13500 days is also plotted.

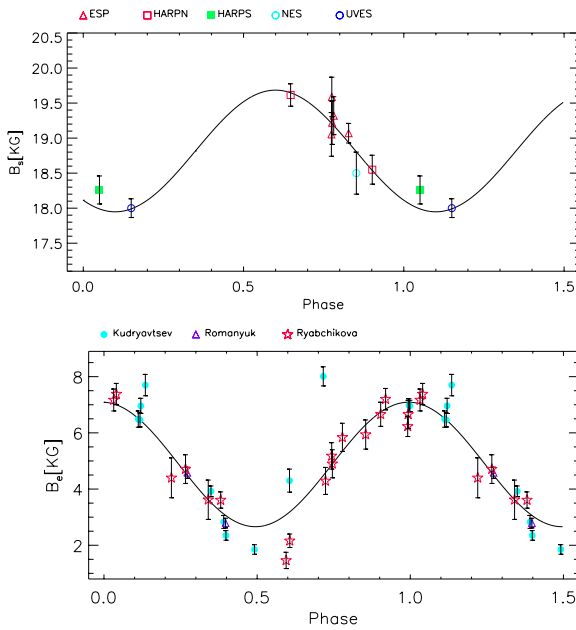


Figure 33. HD 178892: B_s and B_e variability, folded with the 8.2572 d period.

8.2549 days. We retrieved 1 HARPS spectrum, 67 UVES spectra obtained between JD = 2455 351.334 and JD = 2455 351.396 (which subsequently we combined into a single spectrum), 1 NES spectrum and 5 ESPaDOns spectra. In addition, we observed this star twice with HARPS-North. Measured values of B_s are listed in Table 34.

The Lomb-Scargle analysis of our B_s measurements and B_e data from Ryabchikova et al. (2006), Kudryavtsev & Romanyuk (2012) and Romanyuk et al. (2017) results in a $LS(B_s, B_e)$ with a peak at 8.2572 ± 0.0016 d. Figure 33 displays the folded B_s and B_e variations.

3.30 HD 187474

Mathys (1991) established a variability period of 2345 d for HD 187474 from B_s measurements collected in the interval from JD = 2447 287 to 2451 084 (~ 10 yr), and B_e measurements obtained between JD = 2436 002 and 2447 280 (~ 31 years). We have acquired high-resolution spectra of HD 187474 twice with UCLES and twice with HARPS, extending the B_s time coverage (Table 35) by more than 27 years. We have also observed HD 187474 with

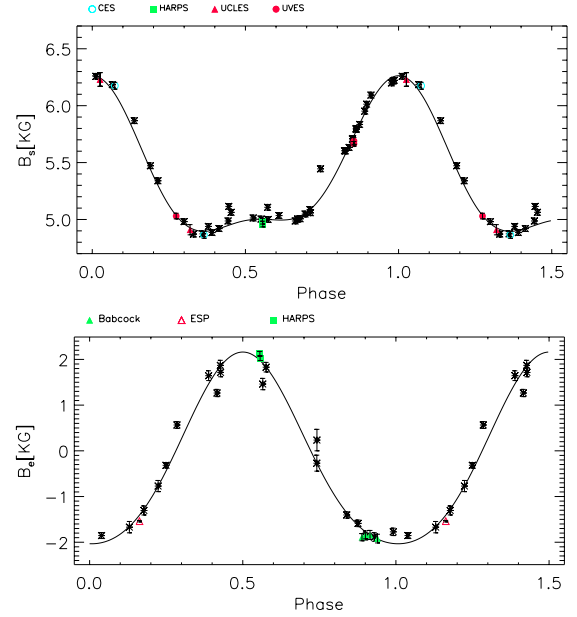


Figure 34. HD 187474. B_s and B_e variability, folded with the 2324 d period.

the HARPS polarimeter – see González et al. (2014) for details – obtaining 2 measurements of B_e :

HJD	B_e
2 456 143.760	2125 ± 50 G
2 456 145.685	2025 ± 50 G

The periodogram of our B_s measurements together with those from M17, and the periodogram of B_e measurements by Babcock (1958), Mathys (1991), Mathys & Hubrig (1997), M17, Sikora et al. (2019) and by us result in a $LS(B_s, B_e)$ function with the highest peak at 2324 ± 40 d. Fig. 34 shows the folded B_s and B_e measurements.

An almost constant surface field of some 5 kG is observed during those phases (from 0.3 to 0.7) where the longitudinal field changes from zero to +2 kG and then back to zero. When the surface field increases from 5 kG to reach a maximum at 6.3 kG, the longitudinal field turns negative, attaining -2 kG (variability phase from 0.7 to 1.3).

3.31 HD 188041

Mikulášek et al. (2003) determined the photometric, magnetic and spectroscopic period of HD 188041 to 223.826 ± 0.040 d. This period has been adopted by P17 for their photometric data but from B_e measurements (covering 50 years), M17 concluded on 223.78 ± 0.10 d. We have observed this stars since JD = 2451 826.349 with SARG, UCLES, CAOS and HARPS-North. Our B_s measurements listed in Table 35 extend the time coverage from 2711 days (7.4 yr) (Mathys 2017) to 10249 days (28 yr). The B_e measurements found in the literature come from Babcock (1954, 1958), Wolff (1969), Mathys (1991), Mathys et al. (1997), M17, and Sikora et al. (2019). The resulting $LS(B_s, B_e)$ presents a peak at 223.82 ± 0.32 d. The poor precision of the period determination is a consequence of the very low amplitude of the B_s variability. In fact, the average value is $\langle B_s \rangle = 3620 \pm 55$ G where the r.m.s. is comparable to the typical error in these measurements. Figure 35 displays the B_s and the B_e data, folded with the period given by

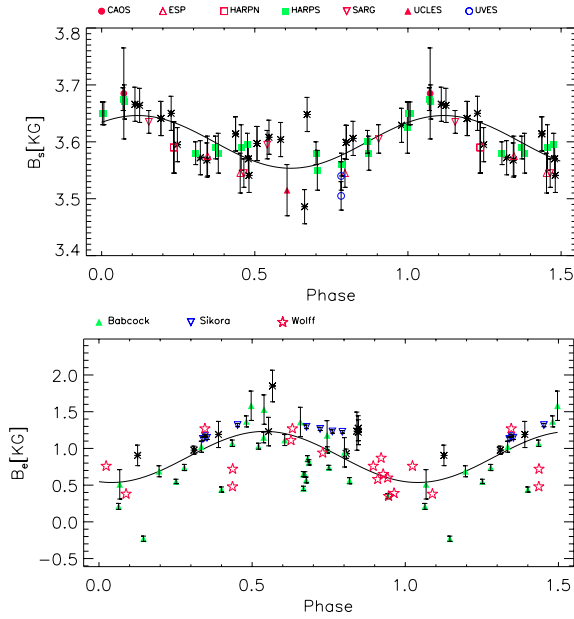


Figure 35. HD 188041. B_s and B_e variability, folded with the 223.826 d period.

Mikulášek et al. (2003). It seems that the B_s maximum coincides with the B_e minimum.

3.32 HD 192678

Pyper & Adelman (2017) found the period of 6.4193 d representative of the photometric and magnetic variability exhibited by HD 192678. The same period was adopted by M17 to discuss the B_s variations of this star. However, this author has pointed out that the B_e measurements by Wade et al. (1996a) do not show any variability with this period. Bychkov et al. (2005) suggested that B_e follows a period equal to 12.91049 d.

To determine the variability period of HD 192678, we have measured B_s from our 2 SARG, 5 CAOS and 2 HARPS-North spectra together with one GECKO archive spectra (Table 37), and we have retrieved TESS photometric data. A Lomb-Scargle analysis of TESS photometry rules out the 12.91049 d period. We have adopted the maximum of $LS(B_s, TESS)$ at 6.4199 ± 0.0001 d as the variability period (Fig. 36). In the same figure we show the folded B_e measurements by Babcock (1958) and Wade et al. (1996a) which however suffer from considerable scatter.

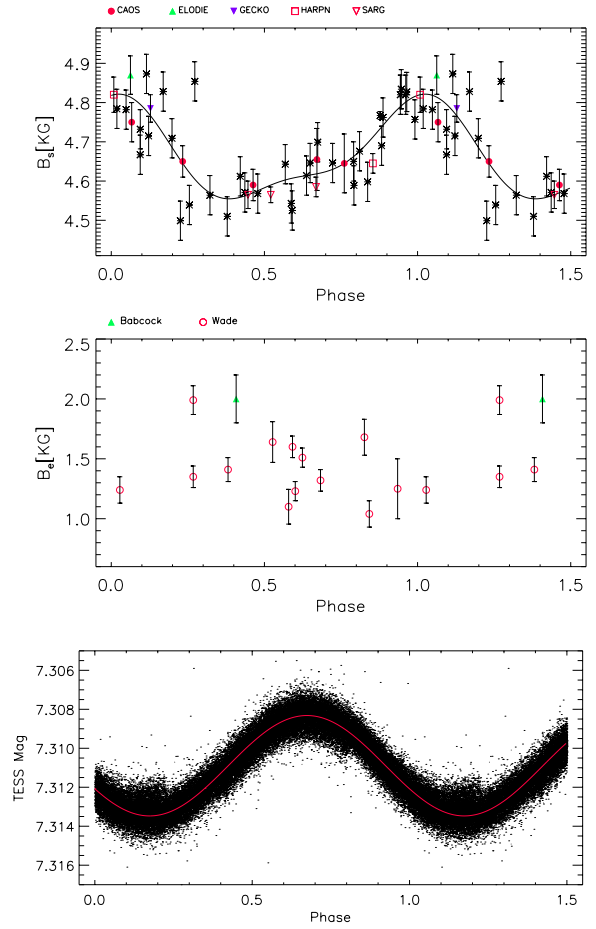


Figure 36. HD 192678. B_s and TESS photometric variability, folded with the 6.4199 d period. B_e measurements by Babcock (1958) and Wade et al. (1996a) show no clear evidence of variability with this period.

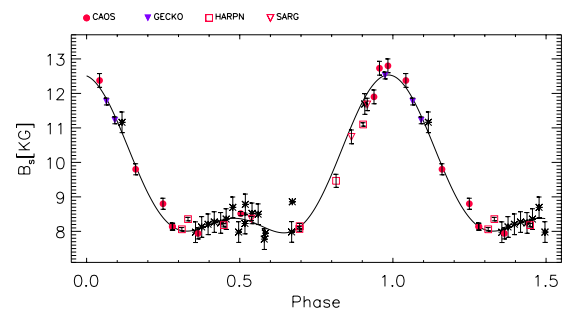


Figure 37. HD 335238. B_s variability, folded with the 48.985 d period.

3.33 HDE 335238

M17 established a variability period of 48.7 ± 0.1 d from B_s measurements. Most of these data were clustered near the minimum value with only two points shaping the B_s maximum. We have observed this star with SARG (3 spectra), CAOS (10) and HARPS-North (6). We also have recovered 3 spectra from GECKO. A Lomb-Scargle analysis of our 22 (Table 38) data points, together with those from M97 (16) and M17 (2) produces a periodogram with the highest peak at 48.985 ± 0.007 d. Fig. 37 shows the B_s measurements, folded with this period.

3.34 HD 201601

The most recent estimate, based on the assumption of a simple sine variation of B_e , of the magnetic variability period of HD 201601 has yielded 97.16 years (Bychkov et al. 2016). We have acquired high-resolution spectra of HD 201601 over 24 years with CES (1 spectrum), SARG (8), UCLES (1), HARPS (2), CAOS (14), HARPS (2), and HARPS-North (10). In addition, 58 spectra have been obtained from ESO, CFHT and TBL archives. Measured values of B_s are listed in Table 39. In order to extend the time interval of the B_s data as much as possible, we have mined the available litera-

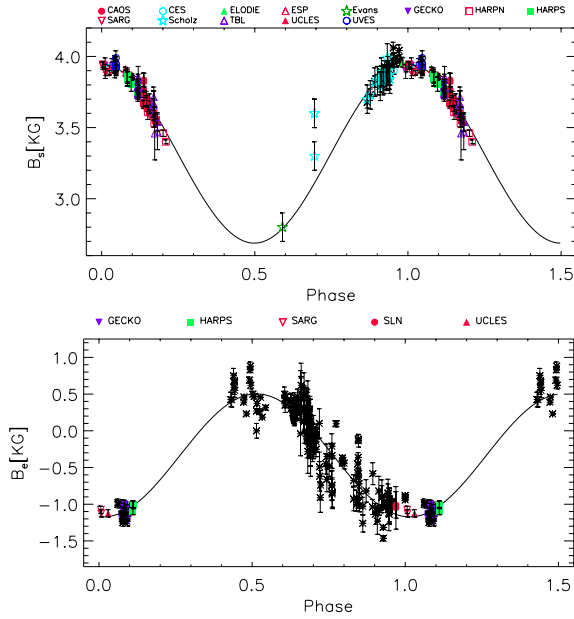


Figure 38. HD 216018. B_s and B_e variability, folded with the 97.16 yr period determined by Bychkov et al. (2016).

ture and found measurements and estimations, also listed in Table 39 together with the appropriate references. We have folded these B_s measurements plus data from Evans & Elste (1971) and Scholz (1979) with the period given by Bychkov et al. (2016). We establish the B_s maximum at JD = 2452 200, and observe a peak-to-peak variation of at least 1.3 kG. From the large number of B_e measurements reported in the literature, we present a sample well distributed in time from the first measurements by Babcock (1958) to the present day (Fig. 38). Folding the data with the period of Bychkov et al. (2016), the B_e minimum appears to coincide with the B_s maximum. Just like we found in the case of HD 116114, HD 165474 or HD 177765, this period is the shortest possible one.

3.35 HD 208217

M17 found the B_s measurements of HD 208217 – collected between JD = 2 449 213 and 2 451 085 – to be variable with the period of 8.44475 d, photometrically determined by Manfroid & Mathys (1997). From TESS photometry, David-Uraz et al. (2019) determined a period equal to 8.317 ± 0.001 d. We have obtained 2 UVES spectra and 8 HARPS spectra from the ESO archive and acquired a new spectrum with HARPS, extending the time coverage to 6932 days. B_s measurements are listed in Table 40. Additionally, we have retrieved TESS photometric data. A Lomb-Scargle analysis gives $LS(B_s, B_e, TESS)$ with a peak at 8.445 ± 0.005 d. Figure 39 shows the variations in B_s , B_e (M17) and TESS.

3.36 HD 216018

From spectra collected between 1992 and 1998, M17 concluded that the period of the variability of HD 216018 – provided there is any periodicity – exceeds 6 years. Table 41 lists our measurements of B_s from 3 UCLES, 2 SARG, 2 HARPS, 3 CAOS, and 3 HARPS-North spectra collected between 2001 and 2018. These plus the M17 measurements result in an average of $B_s = 5600 \pm 45$ G. Computing the Lomb-Scargle periodograms of all B_s data and B_e

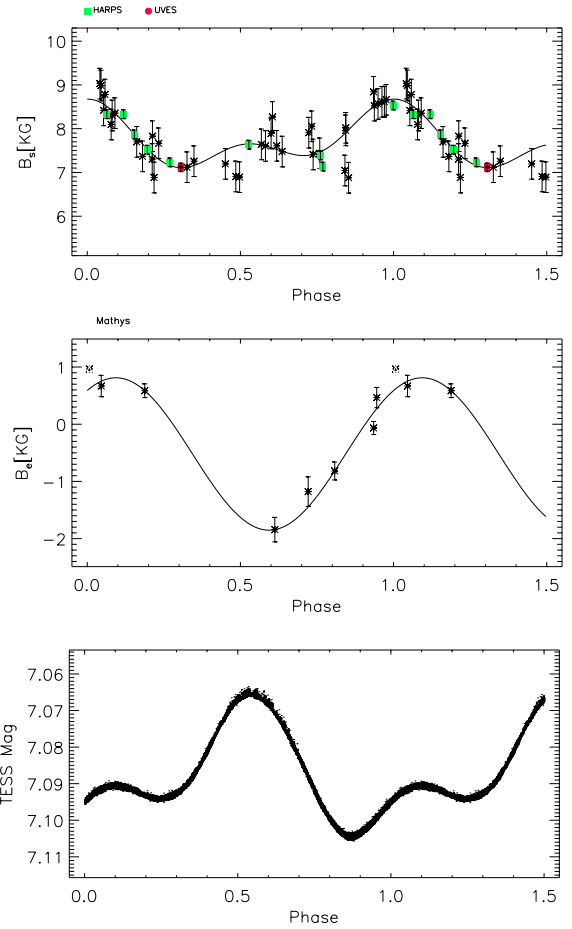


Figure 39. HD 208217. Variations in B_s , B_e and TESS photometry, folded with the 8.445 d period.

measurements by M17 and Romanyuk et al. (2016), we find the main peak of $LS(B_s, B_e)$ at 34.044 ± 0.007 d. Figure 40 displays the folded B_s and B_e data. Both the B_s and B_e variabilities present rather modest amplitudes.

4 MAGNETIC FIELD STRENGTH AND ROTATION PERIOD

Figure 41 shows the average surface field versus the rotation period for the stars discussed above, plus HD 59435, HD 65339, HD 70311, HD 116458 and HD 200311, taken from M17. To highlight possible relationships between periods, field strengths, temperatures and stellar radii (with these two last parameters taken from Gaia Collaboration et al. (2018) for homogeneity), colours indicate temperatures and circles around the position of the star are proportional in size to the stellar radius; radii range from $1.66 R_\odot$ (e.g. HD 154708) to $10.47 R_\odot$ (HD 59435). Such unexpectedly large values for stellar radii are probably a consequence of unresolved components in a binary system or of very small orbital motion perturbing the radius determination. HD 59435 for example is a SB2 system (Wade et al. 1996b).

It appears there is a general decrease of field strength with the period length of stellar rotation. Even though it is probably safe to state that the top-right corner is empty (the result of the Kolmogorov-Smirnov test by M17 has shown that only stars with

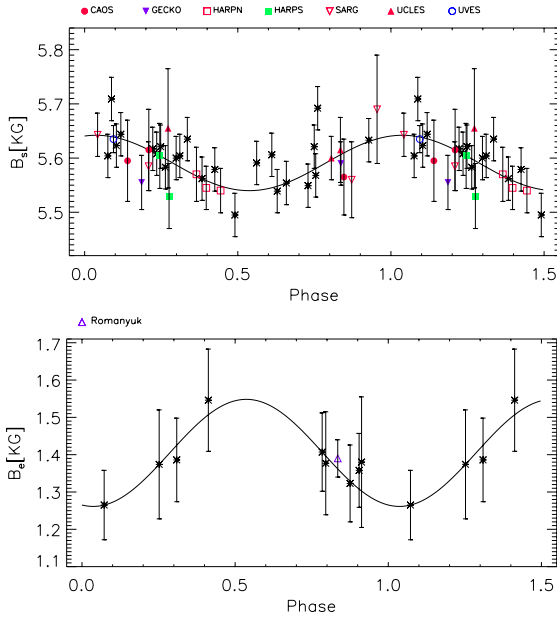


Figure 40. HD 216018. B_s and B_e variability, folded with the 34.044 d period.

rotational periods shorter than 150 days present B_s larger than 7500 G), doubts persist as to the left-bottom corner of Figure 41. It is in fact not possible to measure weak surface fields from the splitting of the FeII 6149.258 Å Zeeman subcomponents when these are considerably broadened by stellar rotation. It would certainly be worthwhile to look at near-infrared lines, given the λ^2 dependence of Zeeman splitting,

The spread for a given value of the period cannot be attributed entirely to the random distribution of angles between line-of-sight, rotation axis and a possible magnetic symmetry axis. For a centred magnetic dipole, the ratio between the largest and smallest values of B_s is only 1.2 (Preston 1969). M17 has observationally shown that for some stars this ratio rises to 2, and here we find that HD 9996 presents $q \sim 3.3$.

5 CONCLUSIONS

The surface field of 36 magnetic chemically peculiar stars has been monitored for 20 years. For every star, by adding archive and literature data, we have extended the time base as much as possible with the aim to determine periods of the order of several decades. Magnetic fields have been derived via the distance in wavelength of the Zeeman subcomponents of the FeII 6149.258 Å line under the hypothesis of linear Zeeman splitting. For a number of stars, magnetic fields are so strong that the partial Paschen-Back effect should be taken into account (Stift et al. 2008). The fact that in these cases we still use the linear approximation does not affect the determination of the period, but rather only concerns the shape of the variability, with amplitudes being underestimated.

In summary: we confirm the rotational periods given in the literature for HD 965, HD 50169, HD 126515 and HD 166473. We select the correct rotational periods among possible values quoted in the literature for HD 2453, HD 9996, HD 81009 and HD 188041. We revisit the periods of HD 12288, HD 14437, HD 18078, HD 51684, HD 61468, HD 93507, HD 94660, HD 142070, HD 144897, HD 154708, HD 318107, HD 178892, HD 187474,

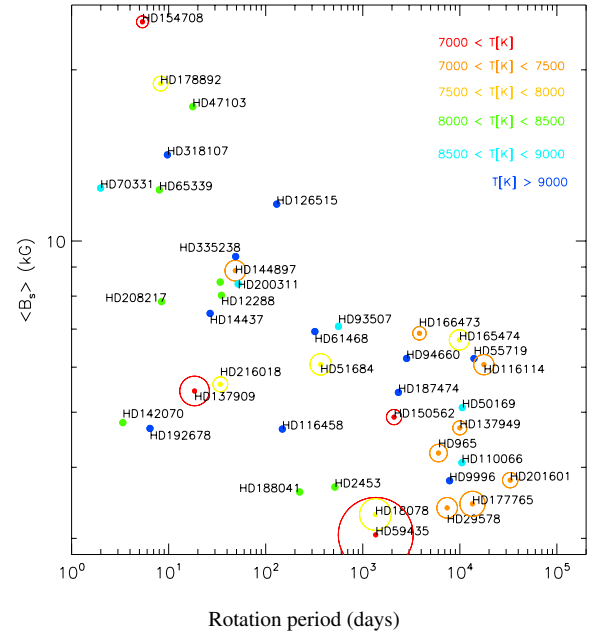


Figure 41. Average surface magnetic field as a function of the rotation period. Colours of filled circles indicate the stellar temperature. Open circles are plotted with radii proportional to the stellar radius, taken from Gaia Collaboration et al. (2018) when available. These radii range from 1.66 R_\odot (e.g. HD 154708) to 10.47 R_\odot (HD 59435).

HD 192678, HD 335238 and HD 208217. To our knowledge, the periods of variability of HD 29578, HD 47103, HD 150562 and HD 216018 have been established here for the first time. Lower limits have been estimated or revised for the variability periods of HD 55719 ($P > 38$ yr), HD 75445 ($P \gg 14$ yr), HD 110066 ($P \gg 29$ yr), HD 116114 ($P > 48$ yr), HD 137949 ($P > 27$ yr), HD 165474 ($P > 27$ yr) and HD 177765 ($P > 37$ yr). It has to be noted that HD 75445 and HD 110066 show no evidence of B_s variability at all.

Concerning γ Equ (= HD 201601), one of the best known magnetic stars, we have pointed out a clear decrease in the surface field over the last 20 years. Despite the fact that the 97 yr period comes from the most extended time series for both B_e and B_s for this class of stars, it could still constitute a lower limit to the rotational period. It appears that the maximum of the surface field has been in phase coincidence with the negative extremum of the longitudinal field.

The results are summarised in Figure 41, plotting the average surface field versus the rotation periods or their lower limits as determined in this study. As a general rule, it seems that longer periods imply weaker fields.

ACKNOWLEDGEMENTS

Our grateful thanks go to the referee, Dr. Gauthier Mathys, for the careful reading and numberless suggestions. Based on observations collected at the European Southern Observatory (ESO) and on data obtained from the ESO Science Archive Facility. Based on observations made with the Italian Telescopio Nazionale Galileo (TNG). The TNG is operated on the island of La Palma by the Fundación Galileo Galilei of the INAF (Istituto Nazionale di Astrofisica) at the Spanish Observatorio del Roque de los Muchachos of the Instituto

de Astrofísica de Canarias”. This paper includes data collected by the TESS mission which are publicly available from the Mikulski Archive for Space Telescopes (MAST). Funding for the TESS mission is provided by the NASA’s Science Mission Directorate. We also acknowledge financial contributions from the agreement ASI-INAf n.2018-16-HH.0 and from the *Programma ricerca di Ateneo UNICT 2020-22 linea 2*.

DATA AVAILABILITY

The spectroscopic data underlying this article are available in the AAT, BTA, CFHT, ESO, TBL and TNG archives at: <https://datacentral.org.au/archives/aat/>
<https://www.sao.ru/oasis/cgi-bin/fetch?lang=en>
<https://www.cadc-ccda.hia-ihp.nrc-cnrc.gc.ca/en/cfht/>
http://archive.eso.org/eso/eso_archive_main.html
<http://polarbase.irap.omp.eu/>
<http://archives.ia2.inaf.it/tng/>
 CAOS data will be shared on reasonable request to the corresponding author.
 TESS photometric data are available in <https://archive.stsci.edu/>.

REFERENCES

- Adelman S. J., 2001, *A&A*, **368**, 225
- Babcock H. W., 1949, *The Observatory*, **69**, 191
- Babcock H. W., 1954, *ApJ*, **120**, 66
- Babcock H. W., 1958, *ApJS*, **3**, 141
- Babcock H. W., 1960, *ApJ*, **132**, 521
- Babel J., North P., 1997, *A&A*, **325**, 195
- Bagnulo S., Fossati L., Landstreet J. D., Izzo C., 2015, *A&A*, **583**, A115
- Bailey J. D., Landstreet J. D., Bagnulo S., Fossati L., Kochukhov O., Paladini C., Silvester J., Wade G., 2011, *A&A*, **535**, A25
- Bailey J. D., Grunhut J., Landstreet J. D., 2015, *A&A*, **575**, A115
- Baranne A., et al., 1996, *A&AS*, **119**, 373
- Bernhard K., Hümmerich S., Paunzen E., 2020, *MNRAS*, **493**, 3293
- Bychkov V. D., Bychkova L. V., Madej J., 2005, *A&A*, **430**, 1143
- Bychkov V. D., Bychkova L. V., Madej J., 2016, *MNRAS*, **455**, 2567
- Bychkov V. D., Bychkova L. V., Metlova N. V., Madej J., 2019, in Kudryavtsev D. O., Romanyuk I. I., Yakunin I. A., eds, *Astronomical Society of the Pacific Conference Series Vol. 518, Physics of Magnetic Stars*. p. 76
- Bychkov V. D., et al., 2021, *Astrophysical Bulletin*, **76**, 297
- Catanzaro G., Giarruso M., Leone F., Munari M., Scialia C., Sparacello E., Scuderi S., 2016, *MNRAS*, **460**, 1999
- Cosentino R., Morales-Juberias R., HDDowling T. E., Butler B. J., 2013, *AGU Fall Meeting Abstracts*, pp P21B–1722
- D’Odorico S., 1990, *The Messenger*, **61**, 51
- David-Uraz A., et al., 2019, *MNRAS*, **487**, 304
- Dekker H., D’Odorico S., Kaufer A., Delabre B., Kotzlowski H., 2000, in Iye M., Moorwood A. F., eds, *Proc. SPIE Vol. 4008, Optical and IR Telescope Instrumentation and Detectors*. pp 534–545, doi:10.1117/12.395512
- Elkin V. G., Wade G. A., 1997, in Glagolevskij Y., Romanyuk I., eds, *Stellar Magnetic Fields*. pp 106–109
- Enard D., 1982, in *Instrumentation in Astronomy IV*. pp 232–242, doi:10.1117/12.933460
- Evans J. C., Elste G., 1971, *A&A*, **12**, 428
- Gaia Collaboration et al., 2018, *A&A*, **616**, A1
- Glaspey J., 1993, *User Manual for GECKO The Coude F/4 Spectrograph*, González J. F., et al., 2014, *A&A*, **561**, A63
- Gratton R. G., et al., 2001, *Experimental Astronomy*, **12**, 107
- Hensberge H., 1993, in Dworetsky M. M., Castelli F., Faraggiana R., eds, *IAU Colloq. 138: Peculiar versus Normal Phenomena in A-type and Related Stars*. *Astronomical Society of the Pacific*, p. 547
- Horton A., et al., 2012, *CYCLOPS2: the fibre image slicer upgrade for the UCLES high resolution spectrograph*. *Society of Photo-Optical Instrumentation Engineers (SPIE)*, p. 84463A, doi:10.1117/12.924945
- Hubrig S., et al., 2005, *A&A*, **440**, L37
- Hubrig S., Mathys G., Kurtz D. W., Schöller M., Elkin V. G., Henrichs H. F., 2009, *MNRAS*, **396**, 1018
- Kaufer A., Stahl O., Tubbesing S., Nørregaard P., Avila G., Francois P., Pasquini L., Pizzella A., 1999, *The Messenger*, **95**, 8
- Kudryavtsev D. O., Romanyuk I. I., 2012, *Astronomische Nachrichten*, **333**, 41
- Landstreet J. D., Bagnulo S., Fossati L., 2014, *A&A*, **572**, A113
- Leone F., Catanzaro G., 2001, *A&A*, **365**, 118
- Leone F., Vacca W. D., Stift M. J., 2003, *A&A*, **409**, 1055
- Leone F., et al., 2016, *AJ*, **151**, 116
- Leone F., Scialia C., Gangi M., Giarruso M., Munari M., Scuderi S., Triglio C., Stift M. J., 2017, *ApJ*, **848**, 107
- Manfroid J., Mathys G., 1997, *A&A*, **320**, 497
- Mathys G., 1990, *A&A*, **232**, 151
- Mathys G., 1991, *A&AS*, **89**, 121
- Mathys G., 1994, *A&AS*, **108**, 547
- Mathys G., 2017, *A&A*, **601**, A14
- Mathys G., Hubrig S., 1997, *A&AS*, **124**, 475
- Mathys G., Hubrig S., Landstreet J. D., Lanz T., Manfroid J., 1997, *A&AS*, **123**, 353
- Mathys G., Romanyuk I. I., Kudryavtsev D. O., Land street J. D., Pyper D. M., Adelman S. J., 2016a, *A&A*, **586**, A85
- Mathys G., Romanyuk I. I., Kudryavtsev D. O., Land street J. D., Pyper D. M., Adelman S. J., 2016b, *A&A*, **586**, A85
- Mathys G., Romanyuk I. I., Hubrig S., Kudryavtsev D. O., Landstreet J. D., Schöller M., Semenko E. A., Yakunin I. A., 2019a, *A&A*, **624**, A32
- Mathys G., Romanyuk I. I., Hubrig S., Kudryavtsev D. O., Schöller M., Semenko E. A., Yakunin I. A., 2019b, *A&A*, **629**, A39
- Mathys G., Khalack V., Landstreet J. D., 2020, *A&A*, **636**, A6
- Mayor M., et al., 2003, *The Messenger*, **114**, 20
- Metlova N. V., Bychkov V. D., Bychkova L. V., Madej J., 2014, *Astrophysical Bulletin*, **69**, 315
- Mikulášek Z., Žižňovský J., Zverko J., Polosukhina N. S., 2003, *Contributions of the Astronomical Observatory Skalnaté Pleso*, **33**, 29
- Nielsen K., Wahlgren G. M., 2002, *A&A*, **395**, 549
- Oskina L. M., Ignace R., Leto P., Postnov K. A., 2020, *A&A*, **641**, L8
- Panchuk V., Klochova V., Yushkin M., Naidenov I., 2009, *J. Opt. Technol.*, **76**, 87
- Press W. H., Rybicki G. B., 1989, *ApJ*, **338**, 277
- Preston G. W., 1969, *ApJ*, **158**, 1081
- Preston G. W., 1970, *ApJ*, **160**, 1059
- Preston G. W., 1971, *ApJ*, **164**, 309
- Preston G. W., Wolff S. C., 1970, *ApJ*, **160**, 1071
- Pyper D. M., Adelman S. J., 2017, *PASP*, **129**, 104203
- Romanyuk I. I., Semenko E. A., Kudryavtsev D. O., 2014, *Astrophysical Bulletin*, **69**, 427
- Romanyuk I. I., Semenko E. A., Kudryavtsev D. O., Moiseeva A. V., 2016, *Astrophysical Bulletin*, **71**, 302
- Romanyuk I. I., Semenko E. A., Kudryavtsev D. O., Moiseeva A. V., Yakunin I. A., 2017, *Astrophysical Bulletin*, **72**, 391
- Ryabchikova T., Nesvacil N., Weiss W. W., Kochukhov O., Stütz C., 2004, *A&A*, **423**, 705
- Ryabchikova T., et al., 2006, *A&A*, **445**, L47
- Schöller M., Hummel C. A., Hubrig S., Kurtz D. W., Mathys G., Robrade J., Järvinen S. P., 2020, *A&A*, **642**, A188
- Scholz G., 1979, *Astronomische Nachrichten*, **300**, 213
- Semenko E. A., Kichigina L. A., Kuchaeva E. Y., 2011, *Astronomische Nachrichten*, **332**, 948
- Sikora J., Wade G. A., Power J., Neiner C., 2019, *MNRAS*, **483**, 3127
- Silvester J., Wade G. A., Kochukhov O., Bagnulo S., Folsom C. P., Hanes D., 2012, *MNRAS*, **426**, 1003

- Solanki S. K., 1994, in Rabin D. M., Jefferies J. T., Lindsey C., eds, Vol. 154, *Infrared Solar Physics*. p. 393
- Stibbs D. W. N., 1950, [MNRAS](#), **110**, 395
- Stift M. J., 1975, *MNRAS*, **172**, 133
- Stift M. J., Goossens M., 1991, *A&A*, **251**, 139
- Stift M. J., Leone F., Landi Degl’Innocenti E., 2008, [MNRAS](#), **385**, 1813
- Stift M. J., Hubrig S., Leone F., Mathys G., 2013, in Shibahashi H., Lynas-Gray A. E., eds, *Astronomical Society of the Pacific Conference Series* Vol. 479, *Progress in Physics of the Sun and Stars: A New Era in Helio- and Asteroseismology*. p. 125
- Talens G. J. J., Spronck J. F. P., Lesage A. L., Otten G. P. P. L., Stuik R., Pollacco D., Snellen I. A. G., 2017, [A&A](#), **601**, A11
- Wade G. A., Elkin V. G., Landstreet J. D., Leroy J. L., Mathys G., Romanyuk I. I., 1996a, *A&A*, **313**, 209
- Wade G. A., North P., Mathys G., Hubrig S., 1996b, *A&A*, **314**, 491
- Wade G. A., Donati J. F., Landstreet J. D., Shorlin S. L. S., 2000a, [MNRAS](#), **313**, 851
- Wade G. A., Kudryavtsev D., Romanyuk I. I., Land street J. D., Mathys G., 2000b, *A&A*, **355**, 1080
- Wade G. A., Debernardi Y., Mathys G., Bohlender D. A., Hill G. M., Landstreet J. D., 2000c, *A&A*, **361**, 991
- Wolff S. C., 1969, [ApJ](#), **158**, 1231
- Wolff S. C., 1975, [ApJ](#), **202**, 127
- Wolff S. C., Morrison N. D., 1973, [PASP](#), **85**, 141
- Wraight K. T., Fossati L., Netopil M., Paunzen E., Rode-Paunzen M., Bewsher D., Norton A. J., White G. J., 2012, [MNRAS](#), **420**, 757
- van Leeuwen F., 2007, [A&A](#), **474**, 653
- van den Heuvel E. P. J., 1971, *A&A*, **11**, 461

Table 6. Measured B_s of HD965.

HJD 2400000+	B_s [G]	Sp	HJD 2400000+	B_s [G]	Sp
51691.929	4190 \pm 50	US	53715.568	4160 \pm 50	HS
51740.091	4250 \pm 60	GO	53716.567	4140 \pm 50	HS
51741.038	4240 \pm 60	GO	54336.860	4120 \pm 50	HS
52120.670	4300 \pm 40	SG	54338.796	4230 \pm 50	HS
52190.627	4280 \pm 50	US	54406.585	4230 \pm 40	HS
52420.066	4220 \pm 40	GO	54442.613	4190 \pm 50	HS
52535.699	4290 \pm 50	US	54443.560	4090 \pm 50	HS
52535.715	4310 \pm 50	US	54469.515	4220 \pm 50	US
52535.731	4300 \pm 50	US	54469.539	4190 \pm 50	US
52535.748	4300 \pm 50	US	54469.562	4190 \pm 50	US
52889.653	4350 \pm 40	SG	54469.580	4200 \pm 50	US
53270.110	4260 \pm 50	UC	56147.773	4200 \pm 70	HS
53334.505	4190 \pm 50	HS	56648.343	4190 \pm 60	HN
53581.741	4110 \pm 50	HS	56892.572	4240 \pm 110	CS
53582.764	4160 \pm 50	HS	56980.341	4260 \pm 80	CS
53583.867	4210 \pm 50	HS	57252.556	4300 \pm 120	CS
53661.707	4110 \pm 50	US	57634.482	4270 \pm 150	CS
53711.565	4160 \pm 50	HS	58367.515	4390 \pm 70	CS
53712.595	4150 \pm 50	HS	58432.484	4340 \pm 50	HN
53713.585	4220 \pm 50	HS	58432.495	4300 \pm 50	HN
53714.583	4170 \pm 50	HS	59441.679	4140 \pm 50	HN

Table 7. Measured B_s of HD2453.

HJD 2400000+	B_s [G]	Sp	HJD 2400000+	B_s [G]	Sp
50349.475	3660 \pm 60	EE	54374.379	3590 \pm 30	SG
52121.649	3690 \pm 30	SG	58096.318	3630 \pm 30	HN
52890.562	3610 \pm 30	SG	58135.220	3610 \pm 40	CS
53215.969	3700 \pm 20	GO	58432.554	3680 \pm 30	CS
53662.628	3680 \pm 20	US	59441.749	3670 \pm 20	HN

Table 8. Measured B_s of HD9996.

HJD 2400000+	B_s [G]	Sp	HJD 2400000+	B_s [G]	Sp
51740.074	1700 \pm 20	GO	56964.449	4710 \pm 80	CS
51799.762	1530 \pm 30	SG	57264.629	4780 \pm 100	CS
52121.660	1610 \pm 30	SG	57340.465	4920 \pm 70	HN
52212.668	1350 \pm 40	SG	58096.461	4190 \pm 40	HN
52890.566	1520 \pm 40	SG	58432.605	3310 \pm 60	HN
53215.113	1700 \pm 30	GO	58828.492	2380 \pm 50	HN
54374.395	1630 \pm 20	SG	59441.695	1680 \pm 50	HN
56938.492	4750 \pm 70	CS			

Table 9. Measured B_s of HD12288.

HJD 2400000+	B_s [G]	Sp	HJD 2400000+	B_s [G]	Sp
49614.586	8330 \pm 110	EE	56964.478	8360 \pm 90	CS
52121.691	7520 \pm 50	SG	57290.555	8230 \pm 100	CS
52212.552	8450 \pm 90	SG	57676.762	8180 \pm 100	HN
53216.027	8350 \pm 100	GO	58137.269	7530 \pm 80	CS
56938.528	8450 \pm 90	CS	59441.736	8315 \pm 50	HN

Table 10. Measured B_s of HD14437.

HJD 2400000+	B_s [G]	Sp	HJD 2400000+	B_s [G]	Sp
52121.719	7250 \pm 60	SG	56980.426	7560 \pm 50	CS
56651.438	7140 \pm 50	HN	58137.293	7600 \pm 60	CS
57340.586	6880 \pm 50	HN	58432.641	7210 \pm 40	HN
57425.414	6980 \pm 90	HN	58432.633	7210 \pm 50	HN
57426.383	7010 \pm 170	HN	59441.723	7640 \pm 40	HN
56964.512	6890 \pm 50	CS			

Table 11. Measured B_s of HD18078.

HJD 2400000+	B_s [G]	Sp	HJD 2400000+	B_s [G]	Sp
49614.558	3550 \pm 180	EE	57340.499	2760 \pm 50	HN
51740.120	2960 \pm 50	GO	57426.397	2820 \pm 20	HN
52890.602	3700 \pm 50	SG	57426.408	2850 \pm 20	HN
53216.054	2820 \pm 50	GO	58432.653	3050 \pm 50	HN
56651.484	4380 \pm 130	HN	58432.664	3050 \pm 50	HN
56980.480	3480 \pm 50	CS	59441.708	4310 \pm 20	HN

Table 12. Measured B_s of HD29578.

HJD 2400000+	B_s [G]	Sp	HJD 2400000+	B_s [G]	Sp
52213.813	5340 \pm 50	US	57056.992	2880 \pm 100	UC
54687.869	3440 \pm 50	FS	51600.518	5130	(Ry)
54868.581	3620 \pm 50	FS	51946.528	5540	(Ry)

Table 13. Measured B_s of HD47103.

HJD 2400000+	B_s [G]	Sp	HJD 2400000+	B_s [G]	Sp
49818.318	17650 \pm 100	(BI)	52286.703	16860 \pm 40	US
49818.330	17480 \pm 100	(BI)	56651.634	16730 \pm 110	HN
49819.388	17420 \pm 100	(BI)	57425.473	17070 \pm 80	HN
50119.485	17370 \pm 100	(BI)	57426.463	16710 \pm 140	HN
50349.643	17160 \pm 100	(BI)			

Table 14. Measured B_s of HD50169.

HJD 2400000+	B_s [G]	Sp	HJD 2400000+	B_s [G]	Sp
52242.612	6030 \pm 50	US	54544.631	5180 \pm 50	HS
53333.857	5830 \pm 50	HS	54545.506	5120 \pm 50	HS
53463.496	5780 \pm 50	HS	54717.904	5060 \pm 50	HS
53464.494	5830 \pm 50	HS	54718.910	5140 \pm 50	HS
53714.661	5630 \pm 50	HS	54865.688	5020 \pm 50	HS
53716.633	5590 \pm 50	HS	54866.617	4970 \pm 50	HS
54222.497	5370 \pm 50	HS	54868.697	5000 \pm 50	HS
54223.509	5350 \pm 50	HS	54869.708	4990 \pm 50	HS
54224.523	5330 \pm 50	HS	56651.699	4390 \pm 50	HN
54336.917	5310 \pm 50	HS	56651.665	4420 \pm 50	HN
54338.914	5310 \pm 50	HS	56651.676	4360 \pm 50	HN
54441.674	5230 \pm 50	HS	56651.687	4370 \pm 50	HN
54442.731	5200 \pm 50	HS	57340.620	4350 \pm 50	HN
54443.689	5250 \pm 50	HS	58075.835	4270 \pm 20	US
54443.760	5230 \pm 50	HS	58179.551	4270 \pm 20	US
54543.493	5160 \pm 50	HS	58432.690	4270 \pm 50	HN

Table 15. Measured B_s of HD51684.

HJD 2400000+	B_s [G]	Sp	HJD 2400000+	B_s [G]	Sp
53333.817	6090 ± 20	US	53632.847	6290 ± 20	US
53340.802	6070 ± 20	US	53666.765	6230 ± 20	US
53340.816	6060 ± 20	US			

Table 16. Measured B_s of HD55719.

HJD 2400000+	B_s [G]	Sp	HJD 2400000+	B_s [G]	Sp
52229.841	6120 ± 40	US	56353.861	6000 ± 80	ES
52229.841	6170 ± 40	US	56353.865	5980 ± 60	ES
53334.680	6040 ± 50	HS	56613.111	6010 ± 30	ES
53334.681	6040 ± 50	HS	56962.134	5920 ± 40	ES
53334.682	6010 ± 40	HS	56962.144	5950 ± 40	ES
53463.535	6050 ± 40	HS	56968.144	5890 ± 30	ES
53463.536	5920 ± 40	HS	56968.155	5870 ± 40	ES
53463.537	6010 ± 50	HS	56972.106	5940 ± 40	ES
53464.536	6100 ± 50	HS	56972.116	5920 ± 40	ES
53464.538	6010 ± 40	HS	57022.022	5940 ± 40	ES
53464.539	6040 ± 40	HS	57022.032	5920 ± 40	ES
53582.949	6160 ± 40	HS	57120.801	5920 ± 60	ES
53712.674	6030 ± 30	HS	57120.812	5940 ± 70	ES
53712.678	6040 ± 30	HS	57120.823	5910 ± 40	ES
53715.631	6060 ± 30	HS	57120.831	5870 ± 90	ES
53715.636	6050 ± 30	HS	57325.109	5850 ± 40	ES
54222.581	6040 ± 40	HS	57325.117	5880 ± 40	ES
54222.585	6050 ± 40	HS	57325.128	5890 ± 30	ES
54865.672	5980 ± 30	HS	57328.138	5970 ± 40	ES
54865.677	5910 ± 40	HS	57328.148	5970 ± 40	ES
55229.615	5900 ± 100	FS	57353.089	5920 ± 40	ES
56343.815	5900 ± 50	ES	57353.100	5930 ± 40	ES
56353.857	5940 ± 50	ES			

Table 17. Measured B_s of HD61468.

HJD 2400000+	B_s [G]	Sp	HJD 2400000+	B_s [G]	Sp
57340.717	6260 ± 85	HN			

Table 18. Measured B_s of HD75445.

HJD 2400000+	B_s [G]	Sp	HJD 2400000+	B_s [G]	Sp
51600.623	2920 ± 50	CE	54205.492	2930 ± 20	HS
51945.543	2950 ± 20	CE	54205.546	2920 ± 20	HS
51955.501	2910 ± 20	CE	54205.600	2935 ± 20	HS
52236.838	2990 ± 50	US			

Table 19. Measured B_s of HD81009.

HJD 2400000+	B_s [G]	Sp	HJD 2400000+	B_s [G]	Sp
52237.853	8000 ± 30	US	54635.460	8540 ± 100	HS
53463.579	8520 ± 30	HS	54635.464	8610 ± 90	HS
53464.585	8820 ± 30	HS	54635.467	8650 ± 100	HS
54204.530	7220 ± 90	HS	54864.731	9670 ± 60	HS
54204.562	7250 ± 60	HS	54864.734	9580 ± 70	HS
54204.594	7240 ± 60	HS	54864.737	9580 ± 50	HS
54204.627	7250 ± 90	HS	54865.607	9510 ± 60	HS
54222.569	9460 ± 60	HS	54865.610	9610 ± 50	HS
54222.572	9430 ± 70	HS	54865.613	9600 ± 50	HS
54222.575	9430 ± 60	HS	54867.732	9440 ± 70	HS
54498.604	8650 ± 60	SG	54867.735	9480 ± 70	HS
54543.522	7160 ± 90	HS	54867.739	9420 ± 70	HS
54543.525	7110 ± 90	HS	54869.609	9140 ± 70	HS
54543.528	7110 ± 70	HS	54869.612	9280 ± 80	HS
54544.526	7260 ± 80	HS	54869.616	9260 ± 70	HS
54544.529	7300 ± 80	HS	54870.626	9090 ± 70	HS
54544.532	7210 ± 80	HS	54870.630	9180 ± 70	HS
54545.709	7440 ± 80	HS	54870.633	9130 ± 70	HS
54545.712	7410 ± 80	HS	56707.426	8740 ± 80	CS
54545.715	7470 ± 80	HS	56710.441	8190 ± 110	CS
54633.491	8920 ± 90	HS	56759.570	8370 ± 140	CS
54633.494	8900 ± 90	HS	57340.777	9080 ± 60	CS
54633.498	8930 ± 80	HS			

Table 20. Measured B_s of HD93507.

HJD 2400000+	B_s [G]	Sp	HJD 2400000+	B_s [G]	Sp
52244.849	7240 ± 60	US	54545.554	7200 ± 70	HS
53463.672	7170 ± 60	HS	54545.561	7220 ± 70	HS
53464.662	7240 ± 80	HS	54633.540	7240 ± 50	HS
53464.669	7240 ± 90	HS	54633.547	7320 ± 60	HS
53581.463	7220 ± 30	HS	54635.495	7370 ± 80	HS
53581.471	7200 ± 40	HS	54635.503	7450 ± 60	HS
54222.675	6840 ± 40	HS	54864.763	6650 ± 50	HS
54222.683	6850 ± 40	HS	54864.770	6730 ± 40	HS
54224.700	6860 ± 40	HS	54867.605	6800 ± 40	HS
54224.711	6910 ± 40	HS	54867.612	6780 ± 40	HS
54441.807	7070 ± 40	HS	54869.656	6780 ± 40	HS
54441.815	6960 ± 40	HS	54869.663	6790 ± 40	HS
54442.816	7090 ± 30	HS	54870.646	6720 ± 40	HS
54442.823	7120 ± 30	HS	54870.654	6740 ± 40	HS
54443.816	7070 ± 40	HS	54870.742	6800 ± 40	HS
54443.823	7030 ± 40	HS	54870.750	6750 ± 40	HS

Table 21. Measured B_s of HD94660.

HJD 2400000+	B_s [G]	Sp	HJD 2400000+	B_s [G]	Sp
50824.041	6380 ± 40	UC	54196.964	6320 ± 30	UC
51176.136	6380 ± 20	UC	54198.928	6380 ± 20	UC
51542.171	6330 ± 20	UC	54928.959	6190 ± 60	UC
52031.464	6140 ± 20	US	54975.546	6130 ± 20	HS
52031.466	6170 ± 20	US	54976.536	6170 ± 20	HS
52265.250	6160 ± 40	UC	54982.605	6130 ± 50	HS
53072.664	6150 ± 20	US	55161.232	6050 ± 20	UC
53072.705	6180 ± 20	US	55202.867	6090 ± 30	HS
53707.846	6380 ± 20	US	55701.447	6120 ± 20	HS
53745.174	6400 ± 20	ES	56018.549	6240 ± 20	HS
54188.098	6440 ± 40	UC	56775.604	6370 ± 20	HS

Table 22. Measured B_s of HD110066.

HJD 2400000+	B_s [G]	Sp	HJD 2400000+	B_s [G]	Sp
51686.409	4140 ± 60	EE	56816.402	4000 ± 70	CS
51739.759	4080 ± 30	GO	57131.457	4200 ± 40	CS
52412.498	4100 ± 40	SG	57471.933	4110 ± 50	ES
52419.774	4070 ± 30	GO	57498.902	4110 ± 50	ES
53544.371	4080 ± 40	SG	59183.159	4110 ± 50	ES
54498.670	4100 ± 30	SG	59191.150	4110 ± 40	ES

Table 23. Measured B_s of HD116114.

HJD 2400000+	B_s [G]	Sp	HJD 2400000+	B_s [G]	Sp
50115.761	5940 ± 50	EM	54222.786	6120 ± 20	HS
52296.868	6030 ± 20	US	54223.718	6100 ± 20	HS
52296.870	6050 ± 20	US	54223.722	6110 ± 20	HS
52676.855	6070 ± 20	US	54224.827	6130 ± 30	HS
52676.862	6050 ± 20	US	54224.831	6120 ± 20	HS
52676.866	6070 ± 20	US	54544.591	6120 ± 20	HS
52676.869	6050 ± 20	US	54544.595	6120 ± 20	HS
52676.872	6050 ± 20	US	54545.677	6160 ± 20	HS
53070.761	6090 ± 10	US	54545.681	6150 ± 20	HS
53544.389	6070 ± 30	SG	54633.653	6120 ± 20	HS
53463.725	6100 ± 20	HS	54633.657	6140 ± 20	HS
53463.729	6050 ± 20	HS	54865.822	6140 ± 20	HS
53464.703	6110 ± 30	HS	54865.826	6090 ± 20	HS
53464.707	6070 ± 20	HS	54868.760	6170 ± 30	HS
53581.520	6060 ± 20	HS	54868.764	6150 ± 30	HS
53581.524	6110 ± 20	HS	54998.717	6160 ± 80	SG
53582.544	6120 ± 20	HS	56706.596	6200 ± 30	CS
53582.548	6110 ± 20	HS	56707.567	6260 ± 30	CS
54204.668	6120 ± 30	HS	57131.486	6220 ± 80	CS
54204.724	6120 ± 40	HS	57234.859	6190 ± 90	UC
54204.789	6110 ± 30	HS	57375.286	6300 ± 100	HN
54222.782	6150 ± 20	HS	57587.432	6240 ± 40	HN

Table 24. Measured B_s of HD126515.

HJD 2400000+	B_s [G]	Sp	HJD 2400000+	B_s [G]	Sp
51979.910	14490 ± 50	US	54544.705	15050 ± 50	HS
51979.913	14550 ± 50	US	54544.710	15150 ± 50	HS
53463.772	9340 ± 50	HS	54633.662	9340 ± 50	HS
53463.777	9310 ± 50	HS	54633.667	9320 ± 50	HS
53464.756	9460 ± 50	HS	54635.481	9410 ± 50	HS
53464.761	9400 ± 50	HS	54635.486	9470 ± 50	HS
53544.401	13730 ± 70	SG	54716.476	13240 ± 50	HS
53582.603	9370 ± 50	HS	54716.481	13140 ± 50	HS
53582.608	9430 ± 50	HS	54864.815	11120 ± 50	HS
53583.566	9320 ± 50	HS	54864.820	10750 ± 50	HS
53583.571	9280 ± 50	HS	54865.832	10650 ± 50	HS
54222.818	9950 ± 50	HS	54865.837	10540 ± 50	HS
54222.823	9920 ± 50	HS	54867.823	10330 ± 50	HS
54223.696	9890 ± 50	HS	54867.828	10400 ± 50	HS
54223.701	9920 ± 50	HS	56707.654	9540 ± 70	CS
54224.786	9820 ± 50	HS	56729.579	11660 ± 140	CS
54224.791	9830 ± 50	HS	57131.517	13370 ± 140	CS
54338.495	11540 ± 50	HS	58294.454	12100 ± 70	HN
54338.500	11580 ± 50	HS	58294.447	11990 ± 90	HN
54543.828	15010 ± 50	HS	59191.162	10270 ± 80	ES
54543.833	15030 ± 50	HS			

Table 25. Measured B_s of HD137949.

HJD 2400000+	B_s [G]	Sp	HJD 2400000+	B_s [G]	Sp
51593.835	4700 ± 20	CE	54598.589	4680 ± 30	SG
52331.803	4680 ± 40	US	54599.521	4720 ± 30	SG
52420.829	4680 ± 20	SG	54600.478	4710 ± 30	SG
52535.505	4700 ± 30	US	54867.786	4710 ± 20	HS
52537.509	4680 ± 10	US	54867.791	4710 ± 20	HS
53214.796	4700 ± 30	SG	54869.789	4720 ± 20	HS
53463.817	4670 ± 10	HS	54869.794	4720 ± 20	HS
53464.798	4710 ± 20	HS	54870.862	4710 ± 20	HS
53511.082	4720 ± 30	UC	54870.868	4720 ± 20	HS
53513.126	4700 ± 30	UC	54953.976	4680 ± 10	ES
53544.424	4680 ± 30	SG	54957.878	4690 ± 50	ES
53581.602	4710 ± 10	HS	54962.896	4680 ± 10	ES
53745.190	4700 ± 20	ES	54963.000	4680 ± 10	ES
53836.299	4760 ± 10	UC	55360.557	4720 ± 30	HS
53930.384	4700 ± 30	SG	55361.522	4710 ± 10	HS
53931.389	4690 ± 40	SG	55364.472	4690 ± 20	HS
53932.382	4670 ± 40	SG	55365.500	4690 ± 10	HS
53949.814	4660 ± 10	ES	55368.490	4690 ± 20	HS
53950.739	4680 ± 10	ES	55369.502	4700 ± 30	HS
53951.738	4660 ± 10	ES	55379.483	4670 ± 10	HS
54222.804	4700 ± 20	HS	55382.619	4710 ± 10	HS
54223.702	4720 ± 30	HS	55383.663	4710 ± 10	HS
54336.599	4740 ± 60	HS	56145.514	4730 ± 40	HS
54498.750	4680 ± 30	SG	57189.402	4750 ± 20	CS
54543.859	4710 ± 20	HS	57221.350	4700 ± 40	CS
54544.719	4700 ± 20	HS	58266.543	4730 ± 20	HN
54544.724	4710 ± 20	HS	58267.520	4730 ± 20	HN
54545.764	4680 ± 20	HS	58906.500	4750 ± 50	CS
54545.770	4710 ± 20	HS			

Table 26. Measured B_s of HD142070.

HJD 2400000+	B_s [G]	Sp	HJD 2400000+	B_s [G]	Sp
52331.872	4640 ± 40	US	54336.496	4970 ± 50	HS
52331.875	4680 ± 30	US	54543.716	4850 ± 40	HS
53463.840	4680 ± 30	HS	54543.724	4700 ± 50	HS
53464.825	4750 ± 40	HS	54543.734	4730 ± 50	HS
53464.832	4730 ± 40	HS	54543.867	4750 ± 30	HS
53582.617	4720 ± 40	HS	54543.876	4700 ± 40	HS
53582.625	4720 ± 40	HS	54544.873	4990 ± 50	HS
53583.630	4850 ± 50	HS	54544.882	4960 ± 40	HS
53583.638	4830 ± 50	HS	54545.817	4750 ± 40	HS
54222.731	4750 ± 30	HS	54545.826	4770 ± 50	HS
54222.740	4770 ± 40	HS	54866.834	4740 ± 50	HS
54222.909	4810 ± 40	HS	54866.843	4780 ± 40	HS
54222.918	4900 ± 40	HS	54867.862	4780 ± 40	HS
54223.772	4730 ± 30	HS	54867.871	4810 ± 40	HS
54223.780	4650 ± 50	HS	54869.860	4630 ± 40	HS
54223.905	4650 ± 90	HS	54869.869	4670 ± 40	HS
54224.737	4970 ± 40	HS	57229.330	5000 ± 90	CS
54224.745	4980 ± 40	HS	57234.874	4740 ± 100	UC
54224.892	4980 ± 50	HS	58266.509	4800 ± 30	HN
54224.901	5090 ± 50	HS	58267.497	4930 ± 100	HN
54336.487	4970 ± 50	HS	58267.497	4930 ± 100	HN

Table 27. Measured B_s of HD144897.

HJD 2400000+	B_s [G]	Sp	HJD 2400000+	B_s [G]	Sp
52331.834	8760 ± 50	US	54543.815	9390 ± 40	HS
53463.864	8550 ± 40	HS	54543.820	9390 ± 40	HS
53463.869	8550 ± 40	HS	54633.569	8700 ± 70	HS
53464.863	8570 ± 40	HS	54633.574	8700 ± 70	HS
53464.868	8570 ± 40	HS	54716.503	8530 ± 50	HS
53581.632	9580 ± 50	HS	54716.508	8530 ± 50	HS
53581.637	9580 ± 50	HS	54865.843	8410 ± 50	HS
53583.669	9460 ± 50	HS	54865.848	8410 ± 50	HS
53583.674	9460 ± 50	HS	54866.854	8490 ± 50	HS
54224.653	8760 ± 70	HS	54866.859	8490 ± 60	HS
54224.659	8760 ± 70	HS	54867.850	8500 ± 50	HS
54336.542	8510 ± 50	HS	54867.855	8480 ± 50	HS
54336.549	8510 ± 50	HS	54868.800	8410 ± 60	HS
54338.591	8590 ± 40	HS	54868.805	8410 ± 50	HS
54338.598	8590 ± 40	HS	57234.894	9080 ± 90	UC

Table 28. Measured B_s of HD150562.

HJD 2400000+	B_s [G]	Sp	HJD 2400000+	B_s [G]	Sp
51252.826	4830 ± 50	EM	54865.885	4920 ± 50	HS
53939.497	4960 ± 50	US	54866.873	4880 ± 50	HS
54336.532	5040 ± 60	HS	54867.813	4980 ± 60	HS
54338.582	4880 ± 50	HS	54868.819	4900 ± 50	HS
54544.824	4950 ± 50	HS	54869.819	4980 ± 50	HS
54545.846	4970 ± 50	HS	54870.853	4970 ± 50	HS
54633.744	4970 ± 50	HS	57234.910	4900 ± 50	UC

Table 29. Measured B_s of HD154708.

HJD 2400000+	B_s [G]	Sp	HJD 2400000+	B_s [G]	Sp
53631.580	24330 ± 270	US	54633.582	24770 ± 210	HS
53631.596	24390 ± 280	US	54716.543	23710 ± 230	HS
53631.633	23970 ± 290	US	54868.871	24250 ± 230	HS
53662.508	24910 ± 270	US	54870.814	24650 ± 210	HS
54543.769	24350 ± 220	HS	55021.779	24380 ± 380	FS
54544.833	23620 ± 230	HS	55029.581	24120 ± 430	FS

Table 30. Measured B_s of HD318107.

HJD 2400000+	B_s [G]	Sp	HJD 2400000+	B_s [G]	Sp
53215.872	14590 ± 200	GO	54633.608	14290 ± 150	HS
53463.893	13870 ± 100	HS	54869.845	13750 ± 50	HS
53582.640	13430 ± 40	HS	54870.874	13880 ± 60	HS
53583.688	13530 ± 80	HS	57234.963	13960 ± 200	UC
54223.637	13530 ± 70	HS	57587.444	14670 ± 300	HN
54553.120	13600 ± 60	ES	58295.517	17000 ± 300	HN
54553.150	13620 ± 60	ES	58295.517	17000 ± 300	HN

Table 31. Measured B_s of HD165474.

HJD 2400000+	B_s [G]	Sp	HJD 2400000+	B_s [G]	Sp
53104.452	6800 ± 40	NS	57220.407	6390 ± 70	CS
53601.345	6780 ± 40	NS	57221.375	6390 ± 80	CS
53871.451	6710 ± 50	NS	57222.435	6330 ± 80	CS
54207.848	6700 ± 10	HS	57223.381	6350 ± 60	CS
54963.440	6610 ± 50	NS	57229.452	6220 ± 80	CS
56145.616	6400 ± 40	HS	58294.554	6460 ± 80	HN
57202.477	6280 ± 50	CS	59441.374	6560 ± 40	HN

Table 32. Measured B_s of HD166473.

HJD 2400000+	B_s [G]	Sp	HJD 2400000+	B_s [G]	Sp
52090.459	8170 ± 80	US	54634.852	5730 ± 50	HS
52189.506	8350 ± 70	US	54634.861	5860 ± 50	HS
54336.612	5790 ± 50	HS	54716.623	5770 ± 50	HS
54336.622	5830 ± 50	HS	54716.633	5880 ± 50	HS
54338.630	5720 ± 50	HS	56531.773	8360 ± 80	ES
54338.639	5730 ± 50	HS	56547.732	8340 ± 90	ES
54544.782	5780 ± 40	HS	56813.014	8070 ± 70	ES
54544.791	5760 ± 50	HS	57239.836	7210 ± 50	ES
54545.866	5760 ± 40	HS	57287.712	7180 ± 50	ES
54545.872	5700 ± 40	HS	58642.993	5860 ± 40	ES
54633.767	5760 ± 40	HS	57235.008	7210 ± 70	UC
54633.777	5740 ± 40	HS			

Table 33. Measured B_s of HD177765.

HJD 2400000+	B_s [G]	Sp	HJD 2400000+	B_s [G]	Sp
54687.752	3410 ± 40	FS	57586.569	3530 ± 30	HN
55359.817	3490 ± 30	US	58294.607	3590 ± 30	HN
57235.029	3530 ± 50	UC			

Table 34. Measured B_s of HD178892.

HJD 2400000+	B_s [G]	Sp	HJD 2400000+	B_s [G]	Sp
53871.405	18500 ± 300	NS	53871.405	18500 ± 300	NS
55351.884	18000 ± 140	US	55351.884	18000 ± 140	US
56356.149	19050 ± 310	ES	56356.149	19050 ± 310	ES
56356.160	19590 ± 280	ES	56356.160	19590 ± 280	ES
56356.166	19220 ± 310	ES	56356.166	19220 ± 310	ES
56430.906	19070 ± 140	ES	56430.906	19070 ± 140	ES
56471.808	19320 ± 270	ES	56471.808	19320 ± 270	ES
57587.510	18550 ± 210	HN	57587.510	18550 ± 210	HN
58295.517	19620 ± 160	HN	58295.517	19620 ± 160	HN
53600.561	18260 ± 200	HS			

Table 35. Measured B_s of HD187474.

HJD 2400000+	B_s [G]	Sp	HJD 2400000+	B_s [G]	Sp
50375.159	6180 ± 30	CE	53270.000	4910 ± 50	UC
51051.667	4870 ± 30	CE	56143.760	4990 ± 30	HS
53164.788	5030 ± 30	US	56145.685	4960 ± 30	HS
52189.525	5670 ± 20	US	57235.076	6230 ± 60	UC
52189.526	5690 ± 30	US			

Table 36. Measured B_s of HD188041.

HJD 2400000+	B_s [G]	Sp	HJD 2400000+	B_s [G]	Sp
51826.349	3640 ± 20	SG	54338.672	3580 ± 40	HS
52119.549	3550 ± 30	SG	54374.362	3600 ± 30	SG
52190.600	3510 ± 30	US	54545.899	3580 ± 20	HS
52190.601	3540 ± 30	US	54633.859	3580 ± 20	HS
52889.376	3610 ± 30	SG	54634.808	3550 ± 40	HS
53270.015	3520 ± 50	UC	54716.644	3680 ± 20	HS
53464.884	3600 ± 20	HS	54717.696	3670 ± 30	HS
53581.663	3630 ± 50	HS	56145.652	3590 ± 40	HS
53582.668	3650 ± 20	HS	56507.449	3690 ± 80	CS
53583.716	3650 ± 20	HS	57239.986	3580 ± 40	ES
54204.876	3560 ± 20	HS	57263.823	3550 ± 40	ES
54223.864	3600 ± 20	HS	57564.132	3550 ± 30	ES
54224.862	3580 ± 30	HS	57886.723	3590 ± 50	HN
54336.651	3590 ± 20	HS			

Table 37. Measured B_s of HD192678.

HJD 2400000+	B_s [G]	Sp	HJD 2400000+	B_s [G]	Sp
49620.334	4870 ± 50	EE	57221.522	4750 ± 50	CS
52120.616	4570 ± 20	SG	57222.591	4650 ± 40	CS
52121.564	4590 ± 30	SG	57230.486	4590 ± 40	CS
52890.527	4570 ± 40	SG	57264.497	4650 ± 80	CS
53215.898	4790 ± 40	GO	58266.601	4650 ± 30	HN
56904.409	4660 ± 80	CS	58267.591	4820 ± 50	HN

Table 38. Measured B_s of HD335238.

HJD 2400000+	B_s [G]	Sp	HJD 2400000+	B_s [G]	Sp
51739.542	11770 ± 100	GO	57240.524	7940 ± 160	CS
51740.896	11220 ± 100	GO	57959.548	12380 ± 200	CS
52420.916	12520 ± 100	GO	57611.553	11900 ± 200	CS
52121.622	10740 ± 200	SG	58299.573	12800 ± 200	CS
52889.396	8370 ± 60	SG	58312.588	8800 ± 160	CS
53544.714	11680 ± 180	SG	57587.537	8180 ± 50	HN
56844.590	8140 ± 100	CS	58095.336	9470 ± 190	HN
56893.490	8140 ± 100	CS	58266.621	8060 ± 50	HN
56904.447	8520 ± 60	CS	58267.602	8360 ± 50	HN
57220.548	12730 ± 200	CS	58295.601	11100 ± 50	HN
57230.548	9800 ± 160	CS	58432.375	8070 ± 70	HN

Table 39. Measured B_s of HD201601.

HJD 2400000+	B_s [G]	Sp	HJD 2400000+	B_s [G]	Sp
37476.500	2800 ± 100	Evans	55168.747	3880 ± 20	ES
41180.411	3600 ± 100	Scholz	55406.850	3860 ± 20	ES
41181.410	3300 ± 100	Scholz	55415.600	3810 ± 50	HS
41182.454	3600 ± 100	Scholz	55490.789	3870 ± 20	ES
47283.000	3700 ± 100	Scholz	55517.704	3840 ± 10	ES
47638.000	3730 ± 100	Scholz	55523.729	3860 ± 10	ES
48169.000	3820 ± 100	Scholz	55524.694	3850 ± 20	ES
48479.000	3830 ± 100	Scholz	55530.768	3860 ± 20	ES
48790.000	3790 ± 100	Scholz	56124.801	3810 ± 50	HS
48925.000	3890 ± 100	Scholz	56126.795	3750 ± 50	HS
49102.000	3830 ± 100	Scholz	56148.712	3760 ± 50	HS
49216.000	3840 ± 100	Scholz	56175.495	3730 ± 50	NL
49457.000	3870 ± 100	Scholz	56176.477	3790 ± 40	NL
49577.000	3860 ± 100	Scholz	56182.373	3740 ± 30	NL
49608.000	3990 ± 100	Scholz	56185.408	3790 ± 40	NL
49696.000	3900 ± 100	Scholz	56234.241	3840 ± 40	NL
49829.000	3870 ± 100	Scholz	56238.250	3860 ± 80	NL
49909.000	3840 ± 100	Scholz	56239.237	3780 ± 70	NL
50374.500	3900 ± 30	CE	56251.237	3790 ± 60	NL
51404.518	3960 ± 30	EE	56252.224	3780 ± 40	NL
51740.013	3900 ± 50	GO	56822.587	3670 ± 30	CS
51773.570	3920 ± 30	SG	56829.600	3740 ± 30	CS
52117.649	3940 ± 30	SG	56830.592	3670 ± 30	CS
52118.547	3950 ± 20	SG	56873.544	3670 ± 20	HN
52412.722	3900 ± 50	SG	56881.466	3770 ± 20	CS
52420.042	3940 ± 50	GO	56881.474	3820 ± 60	CS
52463.730	3890 ± 30	SG	56892.403	3840 ± 50	CS
52889.433	3890 ± 20	SG	57180.587	3660 ± 40	CS
52920.569	3920 ± 20	CE	57189.576	3650 ± 20	CS
53214.938	3940 ± 50	GO	57190.580	3650 ± 20	CS
53270.053	3940 ± 20	UC	57192.517	3710 ± 50	CS
53464.922	3930 ± 10	HS	57193.515	3700 ± 30	CS
53508.708	3900 ± 50	SG	57202.542	3640 ± 20	CS
53512.343	3960 ± 50	UC	57235.083	3690 ± 40	UC
53513.268	3940 ± 50	UC	57240.045	3690 ± 40	ES
53515.269	3940 ± 50	UC	57252.503	3670 ± 30	CS
53541.052	3910 ± 20	ES	57340.357	3610 ± 50	HN
53544.690	3940 ± 20	SG	57340.362	3640 ± 30	HN
53581.690	3920 ± 20	HS	57564.136	3670 ± 30	ES
53582.725	3930 ± 10	HS	57575.590	3690 ± 50	CS
53583.743	3920 ± 20	HS	57586.595	3670 ± 20	HN
53631.752	3930 ± 50	US	57587.561	3610 ± 20	HN
53659.599	3990 ± 50	US	57900.725	3590 ± 20	HN
53659.600	3920 ± 50	US	58012.494	3600 ± 30	HN
53659.600	3950 ± 50	US	58036.391	3670 ± 90	NL
53659.601	3930 ± 50	US	58036.392	3600 ± 100	NL
53659.602	3950 ± 50	US	58037.396	3650 ± 110	NL
54753.743	3910 ± 20	ES	58037.397	3720 ± 70	NL
54818.720	3890 ± 20	ES	58060.696	3580 ± 10	ES
54963.124	3880 ± 20	ES	58094.806	3530 ± 30	HN
54975.828	3860 ± 50	HS	58143.240	3460 ± 190	NL
54975.833	3840 ± 50	HS	58266.684	3550 ± 20	HN
54976.828	3850 ± 50	HS	58267.637	3560 ± 40	HN
54976.833	3870 ± 50	HS	58463.222	3470 ± 130	NL
55028.949	3880 ± 20	ES	58464.225	3540 ± 70	NL
55029.049	3880 ± 10	ES	58474.715	3540 ± 20	ES
55110.824	3880 ± 20	ES	59119.381	3460 ± 20	HN
55160.747	3870 ± 20	ES	59441.366	3400 ± 20	HN

Table 40. Measured B_s of HD208217.

HJD 2400000+	B_s [G]	Sp	HJD 2400000+	B_s [G]	Sp
52189.566	7080 ± 60	US	53715.523	8530 ± 100	HS
52189.570	7160 ± 50	US	53716.539	8330 ± 100	HS
53581.711	7870 ± 100	HS	54205.883	8330 ± 100	HS
53582.691	7230 ± 100	HS	54223.891	7520 ± 100	HS
53711.547	7640 ± 100	HS	56145.746	7140 ± 100	HS
53713.520	7390 ± 100	HS			

Table 41. Measured B_s of HD216018.

HJD 2400000+	B_s [G]	Sp	HJD 2400000+	B_s [G]	Sp
52117.670	5690 ± 100	SG	56144.761	5600 ± 60	HS
52120.654	5640 ± 40	SG	56145.791	5530 ± 60	HS
52190.510	5640 ± 30	US	56892.507	5620 ± 80	CS
52420.046	5590 ± 40	GO	57220.589	5570 ± 70	CS
53214.957	5560 ± 50	GO	57230.588	5600 ± 80	CS
53270.083	5600 ± 40	UC	57235.088	5660 ± 110	UC
53271.093	5620 ± 60	UC	57340.376	5570 ± 50	HN
53544.700	5560 ± 70	SG	58294.694	5550 ± 40	HN
53930.653	5590 ± 50	SG	58432.465	5540 ± 40	HN